Table 1 Number of anterior horn cells, vacuoles and LBHIs in the lumbar segments of G1L and G1H mice (values are given as mean ± SEM)

	G1L						G1H		
	90 days	140 days	180 days	230 days	259 ± 6 days	Non-transgenic (260 ± 6 days)	66 days	100 days	115 days
Anterior horn cells	43 ± 1	43 ± 2	39 ± 2	8 ± 3[b]	4 ± 1[b]	41 ± 1	41 ± 2	31 ± 3[c]	14 ± 3[d]
Vacuoles (total)	2,243 ± 151	1,307 ± 188[a]	842 ± 139[a]	314 ± 42[b]	198 ± 115[b]	0	ND	1,832 ± 259	1,078 ± 201
LBHIs	0	0	4 ± 3	44 ± 18[b]	83 ± 6[b]	0	0	11 ± 3	30 ± 6[d]

G1L Mutant SOD1 (G93A) low-copy mouse; *G1H* mutant SOD1 (G93A) high-copy mouse; *SEM* standard error of the mean; *LBHI* Lewy-body-like hyaline inclusion; *ND* not determined
[a] $P < 0.05$ compared with G1L mice at 90 days; [b] $P < 0.05$ compared with G1L mice at 180 days; [c] $P < 0.05$ compared with G1H mice at 66 days; [d] $P < 0.05$ compared with G1H mice at 100 days

intra-neuritic. The LBHIs in the border zone were larger than those in the vacuole-rich area (=intra-nVII). Quantitative analysis of data from the three subregions of the pons demonstrated a preferential localization of LBHIs to the border zone, the area surrounding the nVII (Table 2, $P < 0.01$).

Immunohistochemical analysis of vacuoles in the facial nucleus of G1L mice

Immunohistochemical analysis of vacuoles in the facial nucleus (nVII) showed that abundant tiny cyt-*c*-positive vacuoles appeared at the edge of the nVII at an early stage (Fig. 8a), similar to those in the lumbar segments. As the disease progressed, the vacuoles became larger (Fig. 8b–f) and were distributed throughout the nVII. Thereafter, although their number decreased progressively, a considerable amount of large vacuoles remained in the nVII even at the end stage (Figs. 7b, 8f). The immunoreactivity for cyt-*c* was weaker in the larger vacuoles than in the tiny vacuoles (Fig. 8b). Immunohistochemical staining for mutant SOD1 showed that the rim of the vacuoles was stained at an early stage (Fig. 8c, d). The SOD1 immunoreactivity of the rim increased at 140 days (Fig. 8d). By 180 days, not only the rim, but also the core of the vacuoles became SOD1-positive (Fig. 8e). At the end stage, the SOD1-positive structures inside the vacuoles decreased. Most of the vacuoles, except for those present in axons, showed weak immunoreactivity for SOD1 in their rim. Vacuoles that were almost SOD1-negative were frequently observed (Fig. 8f).

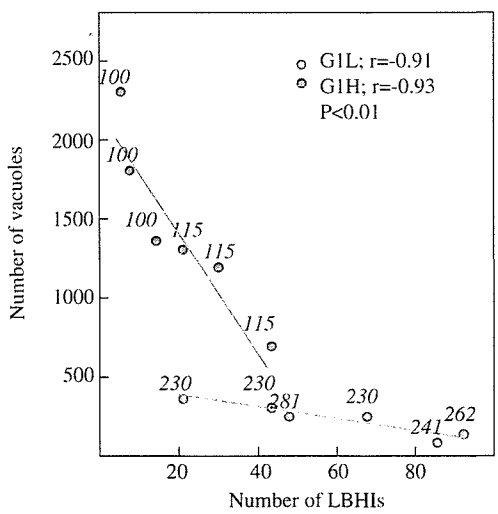

Fig. 6 Inverse correlation between the numbers of mitochondria-derived vacuoles and LBHIs. A statistically significant inverse correlation was observed between the numbers of LBHIs and vacuoles in both G1L (*green*) and G1H (*orange*) mice. Numbers shown in *italics* represent the age of the G93A mice at perfusion

Discussion

In the G93A mouse, the most commonly studied model of ALS, the characteristic neuropathological features are LBHIs and vacuoles [6, 7]. Although scarcely found in FALS patients associated with SOD1 gene mutation [41], it has been considered important to investigate vacuoles [18, 19, 28, 42, 43] because the model mice overexpressing the mutant SOD1 protein could provide clues for understanding the characteristics of mutant SOD1. Also, since evaluation of LBHIs, which are the hallmarks of FALS linked with SOD1 gene mutation, is indispensable for pathological analysis, it is necessary to clarify the factors that can influence their formation.

In control mice, the cytoplasm of the motor neurons showed granular staining with antibodies against subunit I of CCO, a component of the mitochondrion-specific enzyme that is localized in the inner membrane [50], and against cyt *c*, a mediator of CCO that is localized in the intermembrane space [38]. The staining with these antibodies in the motor neurons of control mice corresponds to the localization of mitochondria [11, 19]. In G93A mice, the rims of vacuoles were cyt-*c*-positive and CCO-negative, and the structures lying interior to the vacuolar rim were CCO-positive and cyt-*c*-negative. The latter structures are probably non-functional mitochondrial membrane remnants [14, 28, 43]. Since cyt *c* is released into the cytosol from the permeability transition pores of injured mitochondria [11, 27, 29, 45, 47, 57, 58], the presence of a cyt-*c*-positive

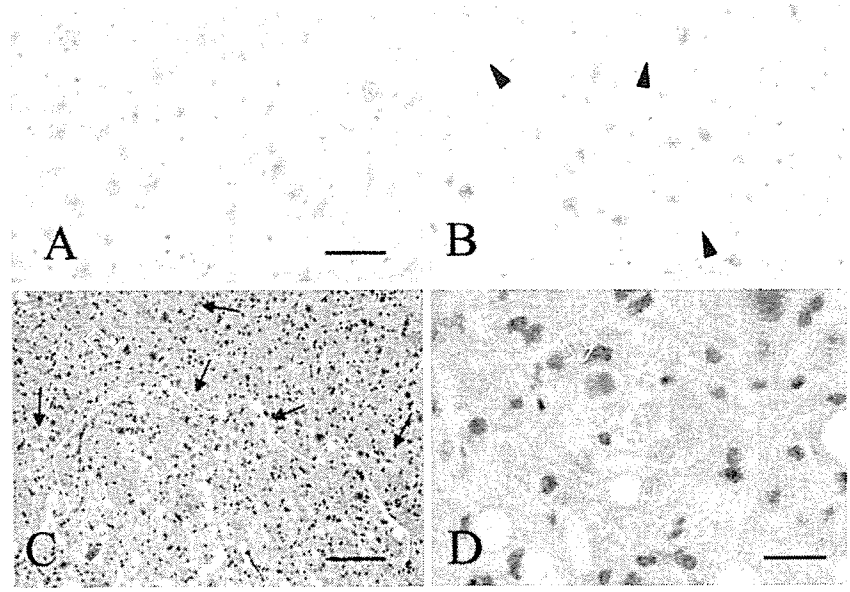

Fig. 7 Representative hematoxylin and eosin staining in the nVII of control (**a**; 261 days) and G1L (**b–d**; end stage) mice. **a**, **b** The number of motor neurons in the G1L nVII is reduced, and all of the residual neurons are atrophic in G1L mice as compared with the controls. Note the prominent vacuolization (*arrow heads*) and lack of LBHIs inside the G1L nVII. **c** Many LBHIs are present (*arrows*, *white arrow*) in the area surrounding the nVII. The *yellow line* delineates the vacuole-rich area (= intra-nVII). **d** A large LBHI (*white arrow*), more than 10 μm in diameter, is located in a neurite, and not in the soma. Scale bar **a** (also for **b**) 50 μm, **c** 100 μm, and **d** 20 μm

rim might imply that cyt *c* is released from the intermembrane space of injured mitochondria into vacuoles to accumulate along the vacuolar rim. Since both small (< 5 μm) and large (> 5 μm) vacuoles in the neuropil exhibited the same immunostaining patterns for cyt *c* and CCO, and since small vacuoles did not appear to fuse to form large ones, it is thought that the small vacuoles grow to become the large vacuoles [14].

According to a previous report, the appearance of vacuoles in the lumbar segments might be related to the onset, rather than progression of the disease, since the number of vacuoles was found to be maximal at disease onset, and declined thereafter [28]. Using antibodies against mitochondrial components, we have shown here that numerous tiny vacuoles, which are distinguishable from cyt-*c*-negative capillary blood vessels, appear in the neuropil approximately 3.5 months before disease onset [14, 19]. In G1L mice, the number of vacuoles in both the lumbar segment and brainstem decreased progressively thereafter, irrespective of disease onset. In contrast with the findings of the previous study [28], therefore, we have found that the presence of these vacuoles appears to be unrelated to disease onset. Although the number of large vacuoles (> 5 μm) increased until disease onset and decreased thereafter, they appeared to be unrelated to disease onset because the degree of neuron loss in the nVII, exhibiting prominent large vacuoles, was much less marked than in the lumbar segment. If the presence of large vacuoles had been related to disease onset, which is determined by neuron loss, then the degree of neuronal loss in the nVII would have been more severe.

In the lumbar segment, intra-neuritic LBHIs appeared just before disease onset and increased rapidly [55] with the progressive reduction in the number of vacuoles in neurites [28, 42, 43]. Although the number of vacuoles was greater in G1H mice than in G1L mice, there was a statistically significant inverse correlation between the number of vacuoles and LBHIs in symptomatic G1L and G1H mice. In the G1L brainstem with prominent vacuole formation, the number of motor neurons was significantly reduced, in agreement with previous reports [13, 35], but only a few LBHIs were found even at the end stage. A notable observation was the presence of many intra-neuritic LBHIs in the border zone where there were few vacuoles. As LBHI formation is known to occur in affected neurons [15, 44, 54], the LBHIs around the nVII would be contained within the neurites of motor neurons in that area. Therefore, there was an inverse correlation between these two neuro-

Table 2 Number of motor neurons and density of LBHIs in the pons divided into three subregions; vacuole-rich area (= intra-nVII), the border zone and vacuole-poor area (values are given as mean ± SEM)

	Age (days)	Number of motor neurons	Density of LBHIs		
			Vacuole-rich area	Border zone	Vacuole-poor area
G1L	258 ± 7	163 ± 8[a]	1.6 ± 0.5[b]	22 ± 8	1.8 ± 0.7[b]
Non-transgenic	264 ± 7	242 ± 3	0	0	0

nVII facial nucleus; *G1L* mutant SOD1 (G93A) low-copy mouse; *SEM* standard error of the mean; *LBHI* Lewy-body-like hyaline inclusion

The density of LBHIs is the number of LBHIs per 1 mm^2 area

[a] $P < 0.05$ compared with non-transgenic mice; [b] $P < 0.01$ compared with border zone

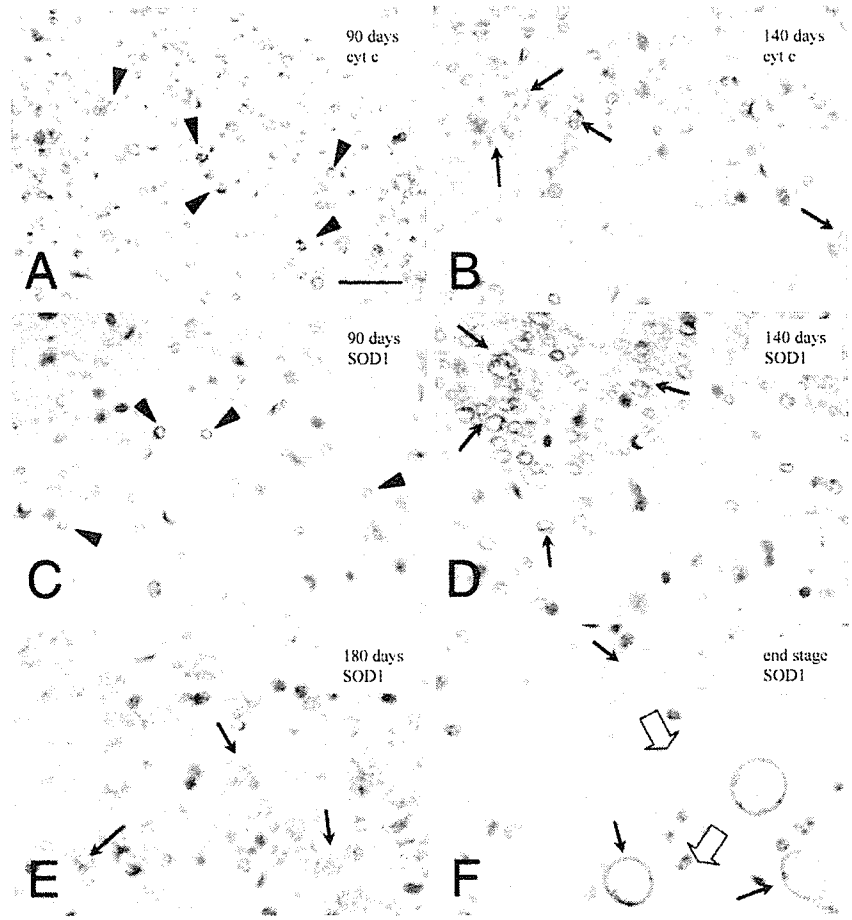

Fig. 8 Immunohistochemical analysis of vacuoles in the nVII of G1L mice (**a**, **c**; 90 days, **b**, **d**; 140 days, **e**; 180 days, **f**; end stage, **a**, **b**; cyt-*c*, **c**–**f**; SOD1). **a** Many tiny cyt-*c*-positive vacuoles (*arrow heads*) are evident. **b** Larger vacuoles (*arrows*) appear, showing lower immunoreactivity than in **a**. **c** Tiny vacuoles (*arrow heads*) are SOD1-positive. **d** SOD1 immunoreactivity becomes stronger at the rim of larger vacuoles (*arrows*) than that of tiny vacuoles observed in **c**. **e** SOD1-positivity is evident not only at the rim, but also the core of the vacuoles (*arrows*). The immunoreactivity has become stronger than that in **d**. **f** Only a few large vacuoles (*arrows*, *clear arrows*) remain. The SOD1 immunoreactivity of vacuoles has become weaker than that in **e**. Some of the vacuoles (*clear arrows*) are almost immunonegative. Scale bar **a** (also for **b**–**f**) 20 μm

pathological changes in both the lumbar segment and the nVII.

Immunohistochemistry using anti-SOD1 antibody revealed that mutant SOD1 accumulated in the rim of tiny vacuoles at an early stage, and was increased in both the rim and the core of the vacuoles [19, 43] until onset. After onset, the intensity of SOD1 immunostaining decreased in both the rim and the core, and SOD1-negative large vacuoles were frequently observed. Since the amount of mutant SOD1 protein increases with age [19, 51], the increased SOD1 immunoreactivity in vacuoles would suggest that more mutant SOD1 was retained in them before onset. The fact that the SOD1 immunoreactivity in vacuoles decreased after onset suggests that vacuoles would not be able to sequester mutant SOD1, despite its higher level of expression in neurons. It is possible that only well-functioning vacuoles at the early stage might be able to retain mutant SOD1. Since mutant SOD1 does not disappear, even when it leaks from vacuoles after onset, it would still remain in the cell [52]. Mutant SOD1 that increased outside vacuoles but remained within the cell would be related to the formation of LBHIs, followed by aggregation of mutant SOD1 in the cell.

In a study using electron and immunofluorescence microscopy, Higgins et al. have reported that the vacuoles originate through expansion of the mitochondrial intermembrane space and extension of the outer mitochondrial membrane and lack lysosomal signals [14]. This suggests that the vacuoles would be produced by a nonautophagic, but still uncharacterized and unique mechanism. In this study, we found a negative correlation between the mitochondria-derived vacuoles and LBHIs, although this does not necessarily mean that the former prevents the latter. However, considering the results of SOD1 immunostaining, it is not unlikely that the mitochondria-derived vacuoles might prevent the formation of LBHIs by sequestering mutated SOD1 from the cytoplasm.

Acknowledgment This study was supported in part by a Health and Labour Sciences Research Grant, Research on Measures for Incurable Disease, Ministry on Health, Labour and Welfare of Japan.

References

1. Barneoud P, Lolivier J, Sanger DJ, Scatton B, Moser P (1997) Quantitative motor assessment in FALS mice: a longitudinal study. Neuroreport 8:2861–2865
2. Bruening W, Roy J, Giasson B, Figlewicz DA, Mushynski WE, Durham HD (1999) Up-regulation of protein chaperones preserves viability of cells expressing toxic Cu/Zn-superoxide dismutase mutants associated with amyotrophic lateral sclerosis. J Neurochem 72:693–699

3. Brujin LI, Becher MW, Lee MK, Anderson KL, Jenkins NA, Copeland NG, Sisodia SS, Rothstein JD, Borchelt DR, Price DL, Cleveland DW (1997) ALS-linked SOD1 mutant G85R mediates damage to astrocytes and promotes rapidly progressive disease with SOD1-containing inclusions. Neuron 18:327–338
4. Brujin LI, Houseweart MK, Kato S, Anderson KL, Anderson SD, Ohama E, Reaume AG, Scott RW, Cleveland DW (1998) Aggregation and motor neuron toxicity of an ALS-linked SOD1 mutant independent from wild-type SOD1. Science 281:1851–1854
5. Cleveland DW, Liu J (2000) Oxidation versus aggregation—how do SOD1 mutants cause ALS? Nat Med 6(12):1320–1321
6. Dal Canto MC, Gurney ME (1994) Development of central nervous system pathology in a murine transgenic model of human amyotrophic lateral sclerosis. Am J Pathol 145:1271–1279
7. Dal Canto MC, Gurney ME (1997) A low expressor line of transgenic mice carrying a mutant human Cu, Zn superoxide dismutase (SOD1) gene develops pathological changes that most closely resemble those in human amyotrophic lateral sclerosis. Acta Neuropathol 93:537–550
8. Deng H-X, Hentati A, tainer JA, Iqbal Z, Cayabyab A, Hung WY, Getsoff ED, Hu P, Herzfeldt B, Roos RP, Warner C, Deng G, Soriano E, Smyth C, Parge HE, Ahmed A, Roses AD, Hallwell RA, Pericak-Vance MA, Siddique T (1993) Amyotrophic lateral sclerosis and structural defects in Cu/Zn superoxide dismutase. Science 261:1047–1051
9. Durham HD, Roy J, Dong L, Figlewicz DA (1997) Aggregation of mutant Cu/Zn superoxide dismutase proteins in a culture model of ALS. J Neuropathol Exp Neurol 56(5):523–530
10. Fischer LR, Culver DG, Tennant P, Davis AA, Wang M, Castellano-Sanchez A, Khan J, Polak MA, Glass JD (2004) Amyotrophic lateral sclerosis is a distal axonopathy: evidence in mice and man. Exp Neurol 185:232–240
11. Guegan C, Vila M, Rosoklija G, Hays AP, Przedborski S (2001) Recruitment of the mitochondrial-dependent apoptotic pathway in amyotrophic lateral sclerosis. J Neurosci 21:6569–6576
12. Gurney ME, Pu H, Chiu AY, Dal Canto MC, Polchow CY, Alexander DD, Caliendo J, Hentati A, Kwon YW, Deng HX, Chen W, Zhai P, Sufit RL, Siddique T (1994) Motor neuron degeneration in mice that express a human Cu, Zn superoxide dismutase mutation. Science 264:1772–1775
13. Haenggeli C, Kato AC (2002) Differential vulnerability of cranial motoneurons in mouse models with motor neuron degeneration. Neurosci Lett 335:39–43
14. Higgins CMJ, Jung C, Xu Z (2003) ALS-associated mutant $SOD1^{G93A}$ causes mitochondrial vacuolation by expansion of the intermembrane space and by involvement of SOD1 aggregation and peroxisomes. BMC Neurosci 4:16
15. Hirano A, Kurland LT, Sayre GP (1967) Familial amyotrophic lateral sclerosis. A subgroup characterized by posterior and spinocerebellar tract involvement and hyaline inclusions in the anterior horn cells. Arch Neurol 16:232–243
16. Howland DS, Jiu J, She Y, Goad B, Maragakis NJ, Kim B, Erickson J, Kulik J, DeVito L, Psaltis G, DeGennaro LJ, Cleveland DW, Rothstein JD (2002) Focal loss of the glutamate transporter EAAT2 in a transgenic rat model of SOD1 mutant-mediated amyotrophic lateral sclerosis (ALS). Proc Natl Acad Sci USA 99:1604–1609
17. Inoue K, Fujimura H, Ogawa Y, Satoh T, Shimada K, Sakoda S (2002) Familial amyotrophic lateral sclerosis with a point mutation (G37R) of the superoxide dismutase 1 gene: a clinicopathological study. Amyotroph Lateral Scler Other Motor Neuron Disord 3:244–247
18. Jaarsma D, Haasdijk ED, Grashorn JAC, Hawkins R, Dujin WV, Verspaget HW, London J, Holstege JC (2000) Human Cu/Zn superoxide dismutase (SOD1) overexpression in mice causes mitochondrial vacuolization, axonal degeneration, and premature motoneuron death and accelerates motoneuron disease in mice expressing a familial amyotrophic lateral sclerosis mutant SOD1. Neurobiol Dis 7:623–643
19. Jaarsma D, Rognoni F, Duijn WV, Verspaget HW, Haasdijk ED, Holstege JC (2001) CuZn superoxide dismutase (SOD1) accumulates in vacuolated mitochondria in transgenic mice expressing amyotrophic lateral sclerosis-linked SOD1 mutations. Acta Neuropathol 102:293–305
20. Johnston JA, Ward CL, Kopito RR (1998) Aggresomes: a cellular response to misfolded proteins. J Cell Biol 143:1883–1898
21. Johnston JA, Dalton MJ, Gurney ME, Kopito RR (2000) Formation of high molecular weight complexes of mutant Cu,Zn-superoxide dismutase in a mouse model for familial amyotrophic lateral sclerosis. Proc Natl Acad Sci USA 97:12571–12576
22. Kato S, Takikawa M, Nakashima K, Hirano A, Cleveland DW, Kusaka H, Shibata N, Kato M, Nakano I, Ohama E (2000) New consensus research on neuropathological aspects of familial amyotrophic lateral sclerosis with superoxide dismutase 1 (SOD1) gene mutations: inclusions containing SOD1 in neurons and astrocytes. Amyotroph Lateral Scler Other Motor Neuron Disord 1:163–184
23. Kato S, Horiuchi S, Liu J, Cleveland DW, Shibara N, Nakashima K, Nagai R, Hirano A, Takikawa M, Kato M, Nakano I, Ohama E (2000) Advanced glycation endproduct-modified superoxide dismutase-1 (SOD1)-positive inclusions are common to familial amyotrophic lateral sclerosis patients with SOD1 gene mutations and transgenic mice expressing human SOD1 with a G85R mutation. Acta Neuropathol 100:490–505
24. Kato S, Sumi-Akamaru H, Fujimura H, Sakoda S, Kato M, Hirano A, Takikawa M, Ohama E (2001) Copper chaperone for superoxide dismutase co-aggregates with superoxide dismutase 1 (SOD1) in neuronal Lewy body-like hyaline inclusions: an immunohistochemical study on familial amyotrophic lateral sclerosis with SOD1 gene mutation. Acta Neuropathol 102:233–238
25. Kato S, Saeki Y, Aoki M, Nagai M, Ishizaki A, Itoyama Y, Kato M, Asayama K, Awaya A, Hirano A, Ohama E (2004) Histological evidence of redox system breakdown caused by superoxide dismutase 1 (SOD1) aggregation is common to SOD1-mutated motor neurons in humans and animal models. Acta Neuropathol 107:149–158
26. Klivenyi P, Ferrante RJ, Mathews RT, Bogdanov MB, Klein AM, Andreassen OA, Mueller G, Wermer M, Kaddurah-Daouk R, Flint Beal M (1999) Neuroprotective effects of creatine in a transgenic animal model of amyotrophic lateral sclerosis. Nat Med 5:347–351
27. Kluck RM, Bossy-Wetzel E, Green DR, Newmeyer DD (1997) The release of cytochrome *c* from mitochondria: a primary site for Bcl-2 regulation of apoptosis. Science 275:1132–1136
28. Kong J, Xu Z (1998) Massive mitochondrial degeneration in motor neurons triggers the onset of amyotrophic lateral sclerosis in mice expressing a mutant SOD1. J Neurosci 18(9):3241–3250
29. Liu X, Kim CN, Yang J, Jemmerson R, Wang X (1996) Induction of apoptotic program in cell-free extracts: requirement for dATP and cytochrome *c*. Cell 86:147–157
30. McHanwell S, Biscoe TJ (1981) The sizes of motoneurons supplying hindlimb muscles in the mouse. Proc R Soc Lond 213:201–216
31. Mohajeri MH, Figlewicz DA, Bohn MC (1998) Selective loss of α motoneurons innervating the medial gastrocnemius muscle in a mouse model of amyotrophic lateral sclerosis. Exp Neurol 150:329–336
32. Nagai M, Aoki M, Miyoshi I, Kato M, Pasinelli P, Kasai N, Brown RH Jr, Itoyama Y (2001) Rats expressing human cytosolic copper-zinc superoxide dismutase transgenes with amyotrophic lateral sclerosis: associated mutations develop motor neuron disease. J Neurosci 21(23):9246–9254
33. Nagano S, Ogawa Y, Yanagihara T, Sakoda S (1999) Benefit of a combined treatment with trientine and ascorbate in familial amyotrophic lateral scledosis model mice. Neurosci lett 265:159–162

34. Nagano S, Satoh M, Sumi H, Fujimura H, Tohyama C, Yanagihara T, Sakoda S (2001) Reduction of metallothioneins promotes the disease expression of familial amyotrophic lateral sclerosis mice in a dose-dependent manner. Eur J Neurosci 13:1363–1370
35. Nimchinsky EA, Young WG, Yeung G, Shah RA, Gordon JW, Bloom FE, Morrison JH, Hof PR (2000) Differential vulnerability of oculomotor, facial, and hypoglossal nuclei in G86R superoxide dismutase transgenic mice. J Comp Neurol 416:112–125
36. Olanow CW, Perl DP, DeMartino GN, McNaught KSP (2004) Lewy-body formation is an aggresome-related process: a hypothesis. Lancet Neurol 3:496–503
37. Paxinos G, Franklin KBJ (2001) The mouse brain in stereotaxic coordinates second edition. Academic Press, Figs 79–85
38. Reed JC (1997) Cytochrome *c*: can't live with it-can't live without it. Cell 91:559–562
39. Ripps ME, Huntley GW, Hoff PR, Morrison JH, Gordon JW (1995) Transgenic mice expressing an altered murine superoxide dismutase gene provide an animal model of amyotrophic lateral sclerosis. Proc Natl Acad Sci USA 92:689–693
40. Rosen DR, Siddique T, Patterson D, Figlewicz DA, Sapp P, Hentati A, Donaldson D, Goto J, O'Regan JP, Deng H-X, Rahmani Z, Krizus A, Mckenna-Yasck D, Cayabyab A, Gaston SM, Berger R, Tanzi RE, Halperin JJ, Herzfeldt B, Van den Bergh R, Hung W-Y, Bird T, Deng G, Mulder DW, Smyth C, Laing NG, Soriano E, Pricak-Vance MA, Haines J, Rouleau GA, Gusella JS, Horritz HR, Brown RH (1993) Mutations in Cu/Zn superoxide dismutase gene are associated with familial amyotrophic lateral sclerosis. Nature 362:59–62
41. Sasaki S, Ohsawa Y, Yamane K, Sakuma H, Shibata H, Nakano R, Kikugawa K, Mizutani T, Tsuji S, Iwata M (1998) Familial amyotrophic lateral sclerosis with widespread vacuolation and hyaline inclusions. Neurology 51:871–873
42. Sasaki S, Warita H, Abe K, Iwata M (2004) Slow component of axonal transport is impaired in the proximal axon of transgenic mice with G93A mutant SOD1 gene. Acta Neuropathol 107:452–460
43. Sasaki S, Warita H, Murakami T, Abe K, Iwata M (2004) Ultrastructural study of mitochondria in the spinal cord of transgenic mice with a G93A mutant SOD1 gene. Acta Neuropathol 107:461–474
44. Shibata N, Hirano A, Kobayashi M, Siddique T, Deng HX, Hung WY, Kato T, Asayama K (1996) Intense superoxide dismutase-1 immunoreactivity in intracytoplasmic hyaline inclusions of familial amyotrophic lateral sclerosis with posterior column involvement. J Neuropathol Exp Neurol 55:481–490
45. Shimizu S, Narita M, Tsujimoto Y (1999) Bcl-2 family proteins regulate the release of apoptogenic cytochrome *c* by the mitochondrial channel VDAC. Nature 399:486–487
46. Stathopulos PB, Rumfeldt JAO, Scholzs GA, Irani RA, Frey HE, Hallewell RA, Lepock JR, Meiering EM (2003) Cu/Zn superoxide dismutase mutants associated with amyotrophic lateral sclerosis show enhanced formation of aggregates in vitro. Proc Natl Acad Sci USA 100(12):7021–2026
47. Steiber A, Gonatas JO, Gonatas NK (2000) Aggregation of ubiquitin and a mutant ALS-linked SOD1 protein correlate with disease progression and fragmentation of the Golgi apparatus. J Neurol Sci 173:53–62
48. Stephens B, Navarrete R, Guiloff RJ (2001) Ubiquitin immunoreactivity in presumed spinal interneurons in motor neurone disease. Neuropathol Appl Neurobiol 27:352–361
49. Sugai F, Yamamoto Y, Miyaguchi K, Zhou Z, Sumi H, Hamasaki T, Goto M, Sakoda S (2004) Benefit of valproic in suppressing disease progression of ALS model mice. Eur J Neurosci 20:3179–3183
50. Tsukihara T, Aoyama H, Yamashita E, Tomizaki T, Yamaguchi H, Shinzawa-Itoh K, Nakashima R, Yaono R, Yoshikawa S (1996) The whole structure of the 13-subunit oxidized cytochrome *c* oxidase at 2.8A. Science 272:1136–1144
51. Turner BJ, Lopes EC, Cheema SS (2003) Neuromuscular accumulation of mutant superoxide dismutase 1 aggregates in a transgenic mouse of familial myotrophic lateral sclerosis. Neurosci Lett 350:132–136
52. Turner BJ, Atkin JD, Farg MA, Zang DW, Rembach A, Lopes EC, Patch JD, Hill AF, Cheema SS (2005) Impaired extracellular secretion of mutant superoxide dismutase 1 associates with neurotoxicity in familial amyotrophic lateral sclerosis. J Neurosci 25:108–117
53. Urushitani M, Kurisu J, Takahashi R (2002) Proteasomal inhibition by misfolded mutant superoxide dismutase 1 induces selective motor neuron death in familial amyotrophic lateral sclerosis. J Neurochem 83:1030–1042
54. Wang J, Xu G, Borchelt DR (2002) High molecular weight complexes of mutant superoxide dismutase 1: age-dependent and tissue specific accumulation. Neurobiol Dis 9:139–148
55. Watanabe M, Dykes-Hoberg M, Culotta VC, Price DL, Wong PC, Rothstein JD (2001) Histological evidence of protein aggregation in mutant SOD1 transgenic mice and in amyotrophic lateral sclerosis neural tissues. Neurobiol Dis 8:933–941
56. Wong PC, Pardo CA, Borchelt DR, Lee MK, Copeland NG, Jenkins NA, Sisodia SS, Cleveland DW, Price DL (1995) An adverse property of a familial ALS-linked SOD1 mutation causes motor neuron disease characterized by vacuolar degeneration of mitochondria. Neuron 14:1105–1116
57. Yamashita S, Mita S, Kato S, Okado H, Ohama E, Uchino M (2003) Bcl-2 expression using retrograde transporter of adenoviral vectors inhibits cytochrome *c*-release and caspase-1 activation in motor neurons of mutant superoxide dismutase 1 (G93A) transgenic mice. Neurosci Lett 350:17–20
58. Yang J, Liu X, Bhalla K, Kim CN, Ibrado AM, Cai J, Peng TI, Jones DP, Wang X (1997) Prevention of apoptosis by Bcl-2: release of cytochrome *c* from mitochondria blocked. Science 275:1129–1132

Available online at www.sciencedirect.com
SCIENCE DIRECT
ELSEVIER
Biochemical and Biophysical Research Communications 343 (2006) 719–730
BBRC
www.elsevier.com/locate/ybbrc

Alteration of familial ALS-linked mutant SOD1 solubility with disease progression: Its modulation by the proteasome and Hsp70

Shingo Koyama [a], Shigeki Arawaka [a,*], Ren Chang-Hong [a], Manabu Wada [a], Toru Kawanami [a], Keiji Kurita [a], Masaaki Kato [b], Makiko Nagai [b], Masashi Aoki [b], Yasuto Itoyama [b], Gen Sobue [c], Pak H. Chan [d], Takeo Kato [a]

[a] *Department of Neurology, Hematology, Metabolism, Endocrinology and Diabetology, Yamagata University School of Medicine, 2-2-2 Iida-nishi, Yamagata 990-9585, Japan*
[b] *Department of Neurology, Tohoku University Graduate School of Medicine, Sendai, Japan*
[c] *Department of Neurology, Nagoya University Graduate School of Medicine, Nagoya, Japan*
[d] *Department of Neurosurgery, Stanford University School of Medicine, Stanford, CA, USA*

Received 9 February 2006
Available online 9 March 2006

Abstract

Accumulation of misfolded Cu/Zn superoxide dismutase (SOD1) occurs in patients with a subgroup of familial amyotrophic lateral sclerosis (fALS). To identify the conversion of SOD1 from a normally soluble form to insoluble aggregates, we investigated the change of SOD1 solubility with aging in fALS-linked H46R SOD1 transgenic mice. Mutant SOD1 specifically altered to insoluble forms, which were sequentially separated into Triton X-100-insoluble/sodium dodecyl sulfate (SDS)-soluble and SDS-insoluble/formic acid-soluble species. In spinal cords, the levels of SDS-dissociable soluble SOD1 monomers and SDS-stable soluble dimers were significantly elevated before motor dysfunction onset. In COS-7 cells expressing H46R SOD1, treatment with proteasome inhibitors recapitulated the alteration of SOD1 solubility in transgenic mice. In contrast, overexpression of Hsp70 reduced accumulation of mutant-specific insoluble SOD1. SDS-soluble low molecular weight species of H46R SOD1 may appear as early misfolded intermediates when their concentration exceeds the capacity of the proteasome and molecular chaperones.

Keywords: Amyotrophic lateral sclerosis; Cu/Zn superoxide dismutase; Heat shock protein; Proteasome; Oligomer

Amyotrophic lateral sclerosis (ALS) is a neurodegenerative disorder characterized by the degeneration of both upper and lower motor neurons, leading to progressive paralysis. Of all ALS cases, ~90% are sporadic and ~10% are familial; ~20% of familial ALS (fALS) cases are associated with dominantly inherited mutations in the gene encoding Cu/Zn superoxide dismutase (SOD1) [1–3]. SOD1 is a major antioxidant enzyme located predominantly in the cytosol, nucleus, and mitochondrial intermembrane space of eukaryotic cells [4]. The biological active enzyme forms a 32-kDa homodimer and contains one copper-binding site and one zinc-binding site, as well as a disulfide bond in each of its two subunits. SOD1-linked fALS was initially suspected to result from oxidative damage caused by diminished SOD1 activity, but SOD1-null mice show no motor neuron disease [5], and transgenic mice overexpressing human mutant SOD1 have a phenotype that is closely similar to patients with fALS, irrespective of their normal or elevated levels of SOD1 activity [6–9]. This evidence indicates that SOD1-linked fALS occurs due to a toxic gain-of-function of mutant SOD1 but not due to a lowering of its activity [6].

Deposition of proteinaceous inclusions of SOD1 in motor neurons is a characteristic hallmark of patients with fALS [10–12]. Cellular and animal models have shown that overexpression of mutant SOD1 can cause loss of motor

* Corresponding author. Fax: +81 23 628 5318.
E-mail address: arawaka@med.id.yamagata-u.ac.jp (S. Arawaka).

0006-291X/$ - see front matter © 2006 Elsevier Inc. All rights reserved.
doi:10.1016/j.bbrc.2006.02.170

neurons with the formation of SOD1-positive inclusions [12–15] and high-molecular-weight (HMW) SOD1 complexes [12,16–19], supporting the hypothesis that the abnormal accumulation of SOD1 aggregates may play a role in the pathogenesis of fALS. Concerning the formation of SOD1 aggregates, several reports have described a close association with the proteasome and heat shock proteins (Hsps). In cells overexpressing mutant SOD1, inhibition of the proteasome activity resulted in the accumulation of insoluble SOD1 protein and the formation of HMW insoluble complexes [16,17,19–22]. On the other hand, Bruening et al. [23] reported that overexpression of Hsp70 reduced aggregate formation and prolonged cellular viability in cells expressing mutant SOD1. These data imply that the conversion of SOD1 from an inherently soluble form to an aggregated species is promoted by insufficiency of the proteasome and/or molecular chaperones, which suppress the accumulation of misfolded proteins. However, the formation of protein aggregation is a complex process, which contains several kinds of misfolded intermediates to form amorphous aggregates and fibrils [24]. There is only a little basic information on how mutant SOD1 undergoes the complex process in relation to the system of proteasome and Hsps.

In the present study, we investigated the alteration of SOD1 solubility with aging in fALS-linked mutant H46R SOD1 transgenic mice. We also examined its change in mutant SOD1 expressed cells by treatment with proteasome inhibitors. Furthermore, using cells co-expressing mutant SOD1 and Hsp70, we characterized an insoluble SOD1 species influenced by Hsp70 as misfolded proteins. Here we show that SDS-dissociable soluble monomers and SDS-stable soluble dimers of H46R SOD1 appear as early misfolded intermediates in the formation of highly insoluble aggregates, and their levels are coordinately mediated by the proteasome activity and Hsp function.

Materials and methods

Materials. We used the following antibodies: polyclonal human SOD1 antibody (SOD1-100, diluted 0.1 μg/ml, Victoria, BC, Canada); monoclonal antibody against GST-fused full-length human SOD1 protein that specifically binds to human SOD1 (diluted 0.2 μg/ml, MBL, Nagoya, Japan); polyclonal Hsp70 antibody (SPA-757, diluted 1:30,000 for Western blotting, diluted 1:1000 for immunohistochemistry, Stressgen); polyclonal Hsp40 antibody (SPA-400 diluted 1:10,000 for Western blotting, diluted 1:500 for immunohistochemistry, Stressgen). Wild-type SOD1 cDNA fused with an FLAG tag at C-terminus of SOD1 (SOD1-FLAG) was subcloned into either pcDNA3.1 (Invitrogen, Carlsbad, CA, USA) or pEF-BOS vector [20]. Mutant H46R and G93A SOD1 cDNAs were generated by site-directed mutagenesis, and their sequences were confirmed by DNA sequencing. pCMV-Hsp70 and pRC-Hsp40 were described previously [25,26].

Cell culture and transfection. COS-7 and SH-SY5Y cells were grown in Dulbecco's modified Eagle's medium (DMEM, Invitrogen) and a mixture of DMEM and Ham's F-12, respectively, supplemented with 10% fetal bovine serum. SOD1 cDNAs were transfected into cells using Lipofectamine Plus reagents (Invitrogen), according to the manufacturer's protocols [27]. Cultured cells were harvested 48 h after transfection for experiments. For inhibition of the proteasome activity, either MG132 or lactacystin (Sigma, St. Louis, MO, USA) in indicated concentrations was added to cells 24 h after transfection and then cells were further incubated for 24 h. In experiments using Hsp chaperones, either Hsp70 or Hsp40 cDNA was co-transfected with H46R SOD1-FLAG pEF-BOS to COS-7 cells (at a molar ratio of 4:1).

Transgenic mice. Transgenic mouse lines expressing fALS-linked H46R SOD1 under the control of inherent human SOD1 promoter were maintained as hemizygotes by mating with B6/SJF1 as previously described [28]. The transgenic mice expressing wild-type human SOD1 were also kindly supplied by Dr. PH. Chan (Stanford University, Stanford, CA, USA) and maintained as hemizygotes [29]. All of the mouse experiments followed the Guidelines for Animal Experiments of Yamagata University School of Medicine.

Protein fractionation and Western blotting. Protein fractionation of whole mouse spinal cords was performed according to published protocols [30,31] with a slight modification (see Fig. 1A). Whole mouse spinal cords were homogenized by 15 up-and-down strokes with a Teflon homogenizer in 1:3 (wt/vol) phosphate-buffered saline (PBS; 100 mM phosphate, pH 7.4, 150 mM NaCl, and protease inhibitor cocktail (Roche Diagnostics, Mannheim, Germany)). The homogenate was centrifuged at 100,000×*g* for 20 min at 4 °C, and the resultant supernatant was collected as the PBS-soluble fraction. The pellet was rinsed three times with PBS and was extracted by sonication in 1% Triton X-100 (TX)/PBS. After centrifugation at 100,000×*g* for 20 min at 4 °C, the supernatant was designated as the TX-soluble fraction. The pellet was washed three times with 1% TX/PBS and extracted by sonication in 5% SDS/PBS. The extract was incubated at room temperature for 30 min and centrifuged at 100,000×*g* for 20 min at 20 °C. The supernatant was designated as the SDS-soluble fraction. After rinsing and centrifugating three times in 5% SDS/PBS, the resultant pellet was extracted by sonication in 8 M urea/PBS. After centrifugation at 100,000×*g* for 20 min at 20 °C, the supernatant was designated as the urea-soluble fraction. The pellet was rinsed once with 8 M urea/PBS and extracted by sonication in 88% formic acid (FA). After centrifugation at 100,000×*g* for 20 min at 20 °C, the supernatant was designated as the FA-soluble fraction. FA was evaporated by SpeedVac (Savant, Farmingdale, NY, USA). After washing the dried pellet with distilled water and lyophilizing it again, the resulting pellet was resuspended by sonication in Laemmli's sample buffer containing 2% SDS and 100 mM dithiothreitol and then boiled for 5 min. The protein concentrations of the PBS-soluble, TX-soluble, SDS-soluble, and urea-soluble fractions were measured by a BCA protein assay (Pierce, Rockford, IL, USA). Cultured cell pellets were fractionated by the same protocol described above until the preparation of the SDS-soluble fraction. The SDS-insoluble pellet was resuspended by sonication in Laemmli's sample buffer and boiled for 5 min. The suspension was designated as the SDS-insoluble fraction.

We performed Western blotting as described previously [27]. All protein samples were boiled for 5 min in Laemmli's sample buffer containing 100 mM dithiothreitol. Ten micrograms of protein from each of the PBS-soluble, TX-soluble, SDS-soluble, and urea-soluble fractions, and equal aliquots of the FA-soluble fraction were loaded on 15% polyacrylamide gels. The relative intensities of detected bands were scanned and quantified with the Scion image program, version 4.02 (Scion Corp., Frederick, MD, USA). Statistical analysis for comparison of groups was performed by ANOVA with Fisher's probability of least significant difference (PLSD) post hoc test for significance using the Statview software version 5 (SAS Institute Inc, Cary, NC, USA).

Immunohistochemistry. The mice, anesthetized with diethyl ether, were sacrificed by transcardial perfusion with 0.9% sodium chloride followed by 4% paraformaldehyde in PBS. The spinal cord was quickly removed, post-fixed with the above solution, and then embedded in paraffin. After deparaffinizing, sections (4-μm thickness) of the lumbar spinal cord (L_{4-5}) were incubated with 0.3% hydrogen peroxide for 10 min and then with 10% normal goat serum for 30 min. The sections were incubated with the primary antibodies, and they reacted with the appropriate biotinylated secondary antibodies, followed by an avidin-biotin-peroxidase complex (Vector, Burlingame, CA, USA). Color was developed with diaminobenzidine (Sigma).

Results

Mutant-specific alteration of SOD1 solubility in fALS-linked H46R SOD1 transgenic mice

In this study, we used fALS-linked H46R SOD1 transgenic mice as reported previously [28]. To examine the fALS-linked mutation-dependent change of SOD1 solubility, we sequentially extracted spinal cords of mutant transgenic mice with severe motor impairment (~24 weeks of age) with PBS, 1% TX, 5% SDS, 8 M urea, and 88% FA (Fig. 1A), and then separated extracts by SDS–PAGE under the denaturing condition. In 24-week-old non-transgenic littermates and 38-week-old wild-type SOD1

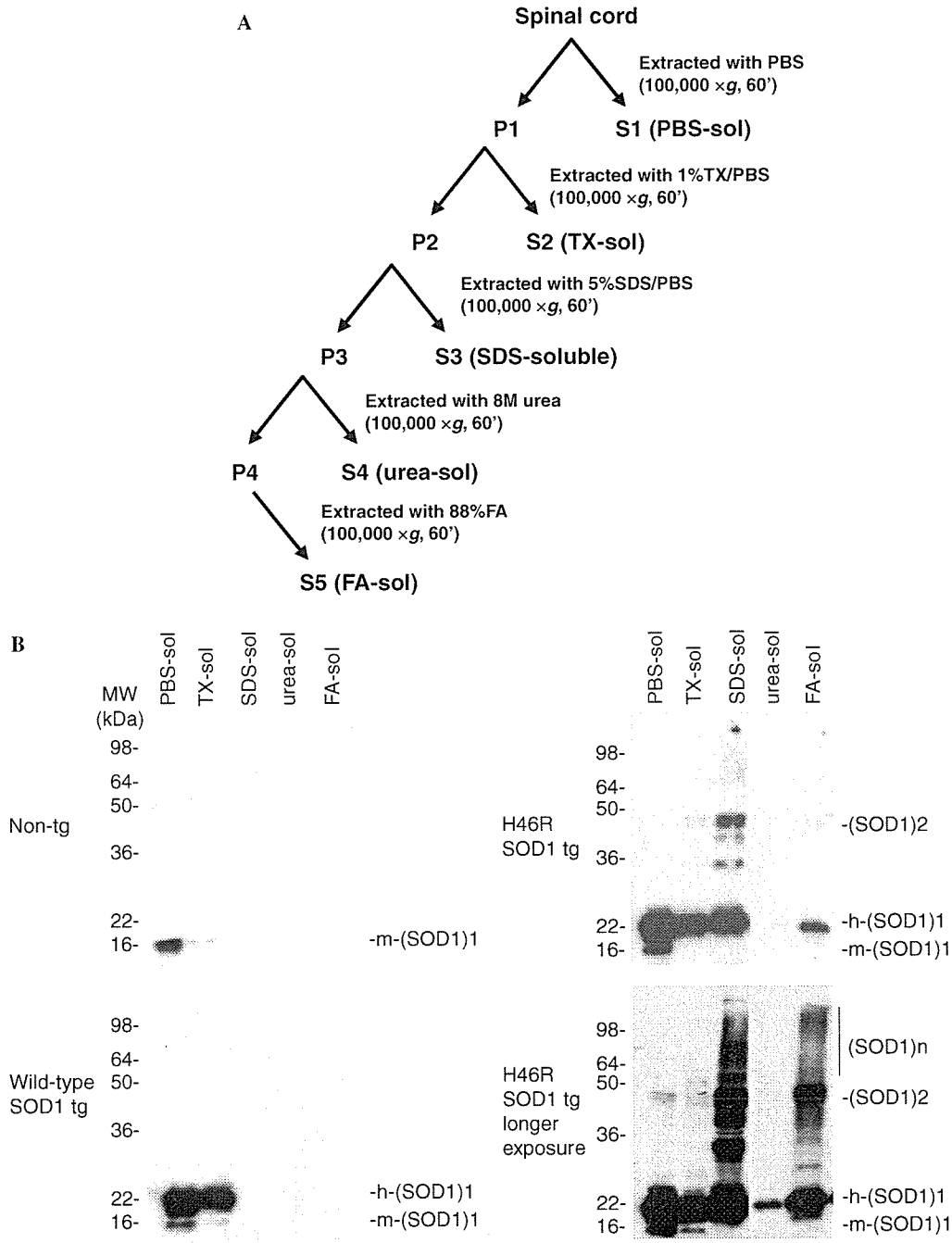

Fig. 1. Mutant-specific alteration of SOD1 solubility in spinal cords from fALS-linked H46R SOD1 transgenic mice. (A) Schematic representation of the sequential extraction steps. (B) Western blot analysis of spinal cords from 24-week-old non-transgenic mice (Non-tg) (upper left panel), 38-week-old wild-type SOD1 transgenic mice (Wild-type SOD1 tg) (lower left panel), and mutant H46R SOD1 transgenic mice at end stage (H46R SOD1 tg) (upper right panel). Ten micrograms of protein from each of the PBS-soluble fraction (PBS-sol), the TX-soluble fraction (TX-sol), the SDS-soluble fraction (SDS-sol), and the urea-soluble fraction (urea-sol) and equal aliquots of the FA-soluble fraction (FA-sol) were subjected to 15% polyacrylamide gels under reducing conditions. Western blots were probed with SOD1-100 antibody, which recognizes both human SOD1 (h-SOD1) and mouse endogenous SOD1 (m-SOD1). The lower right panel (identical to the upper right panel) was exposed to the film for a longer time.

transgenic mice, endogenous mouse SOD1, and wild-type human SOD1 were detected as monomers migrating at 16-kDa and 22-kDa, respectively, in the PBS- and 1% TX-soluble fractions (Fig. 1B). This finding may be explained by the fact that normal SOD1 is a soluble protein located predominantly in the cytosol and less within the membranous organelle such as mitochondrial intermembrane space [4]. In contrast to the control mouse SDS-soluble fraction that was virtually devoid of SOD1, intense bands of SOD1 were found in the SDS-soluble fraction of mutant transgenic mice (Fig. 1B). In the fraction, the anti-SOD1 antibody (SOD1-100) recognized 22-kDa bands ((SOD1)1; it represents SOD1 monomer), ~44-kDa bands ((SOD1)2; apparent molecular weight of (SOD1)2 shows 2-fold to 22-kDa monomer, being consistent with SOD1 dimer as previously reported [19]), and multiple bands above 44-kDa ((SOD1)n; it represents high-molecular-weight (HMW) species). Also, ~28 and ~36-kDa bands were observed in the SDS-soluble fraction. These bands may represent proteolytic fragments from HMW species, but the exact origin was unknown in this study. SOD1 monomers, dimers, and HMW species were further recovered in the FA-soluble fraction, whereas a small amount of monomeric SOD1, but not HMW species, was detected in the urea-soluble fraction, indicating that FA-soluble SOD1 species were not simply carried over from the prior urea extracts (Fig. 1B). TX-insoluble/SDS-soluble (designated as SDS-soluble) species are characterized by an alteration of solubility to distinguish mutant H46R SOD1 from a wild-type one. Also, mutant H46R SOD1 contained SDS-stable oligomers with diverse solubility in detergents or denaturants.

Age-dependent alteration of SOD1 solubility in H46R SOD1 transgenic mice

As described in our previous report, the H46R SOD1 transgenic mice showed motor dysfunction with aging, and the stages of motor dysfunction could be classified into four time periods based on the Rotarod test: 13 weeks, 17 weeks, 21 weeks, and later 23 weeks of age were designated as the early presymptomatic stage (EP), late presymptomatic stage (LP), symptomatic stage (SS), and end stage (ES), respectively [28]. To clarify the alteration of SOD1 solubility with aging in mutant SOD1 transgenic mice, we compared the levels of SOD1 species, which were biochemically fractionated as described above, in the different stages (Figs. 2A and B). The levels of both PBS-soluble and TX-soluble SOD1 monomers showed no statistically significant difference between stages, although they had a tendency to decrease with aging (Figs. 2A and B). In the SDS-soluble fraction, mutant SOD1 monomers and dimers were clearly detected at EP. The ratios of SOD1 monomers at EP and LP versus ES were $20.52 \pm 6.41\%$ (mean $\pm$ SD) and $45.88 \pm 2.30\%$, respectively. In addition, the ratios of SOD1 dimers at EP and LP versus ES were $29.38 \pm 21.20\%$ and $68.47 \pm 10.27\%$, respectively. On the other hand, the levels of SOD1 HMW species showed the later elevation at the period between LP and SS. These findings indicate that the increase of SDS-dissociable soluble SOD1 monomers and SDS-stable soluble SOD1 dimers occurred between EP and LP before onset ($n = 3$, $p = 0.017$ and $p = 0.005$, respectively) (Fig. 2B). In the FA-soluble fraction, a small number of SOD1 monomers were also seen at EP, but there was no significant difference in the levels of monomers between EP and LP. The ratios of SOD1 monomers at LP and SS versus ES were $32.31 \pm 12.99\%$ and $68.30 \pm 17.03\%$, respectively. The ratios of SOD1 dimers at LP and SS versus ES were $12.73 \pm 6.27\%$ and $41.42 \pm 4.50\%$, respectively. The levels of FA-soluble SOD1 monomers and FA-soluble dimers significantly increased between LP and SS ($p = 0.036$ and $p < 0.001$, respectively), while the levels of FA-soluble SOD1 HMW species elevated later in the period between SS and ES (Figs. 2A and B). The levels of SDS-dissociable soluble monomers and SDS-stable soluble dimers elevated earlier than the SDS-stable soluble HMW species and FA-soluble species.

To examine the relation between the alteration of SOD1 solubility and the formation of SOD1-inclusions with aging, we immunostained mouse spinal cords in four different stages with monoclonal anti-SOD1 antibody (Fig. 2C). At EP, we did not detect any kind of SOD1-inclusions. SOD1-inclusions in the neuropil appeared at SS, and the number of SOD1-inclusions increased between SS and ES (Fig. 2C). SOD1-inclusions increased after disease onset, indicating that the accumulation of SDS-dissociable soluble SOD1 monomers and SDS-stable soluble dimers precedes the appearance of SOD1-inclusions.

The increase of Hsp70/40 in the SDS-soluble fraction with aging in H46R SOD1 transgenic mice

To examine how the mutant-specific alteration of SDS solubility is associated with the molecular chaperone system, the fractionated samples prepared above were analyzed by Western blotting using antibodies to Hsp70 and Hsp40. Hsp70 and Hsp40 were found to be rich in the PBS-soluble and the TX-soluble fractions (Fig. 3A). PBS- and TX-soluble Hsp70 and Hsp40 showed constant levels in all stages of mutant transgenic mice and were not different from those in 24-week-old non-transgenic littermates and 38-week-old wild-type SOD1 transgenic mice (Fig. 3A). In the SDS-soluble fraction, the levels of Hsp70 and Hsp40 in mutant transgenic mice at LP were higher than those in the control mice at later 24 weeks of age. The levels of Hsp70 and Hsp40 in the SDS-soluble fractions elevated at the period between EP and LP in mutant transgenic mice (Fig. 3A). To clarify how the increase of Hsp70 and Hsp40 in the SDS-soluble fraction reflects in histopathological change with aging, we immunostained the lumbar spinal cords with antibodies to Hsp70 and Hsp40 (Fig. 3B). SOD1-positive inclusions were intensely stained with the antibody to Hsp70 as previously reported and faintly reacted with the antibody to Hsp40 in

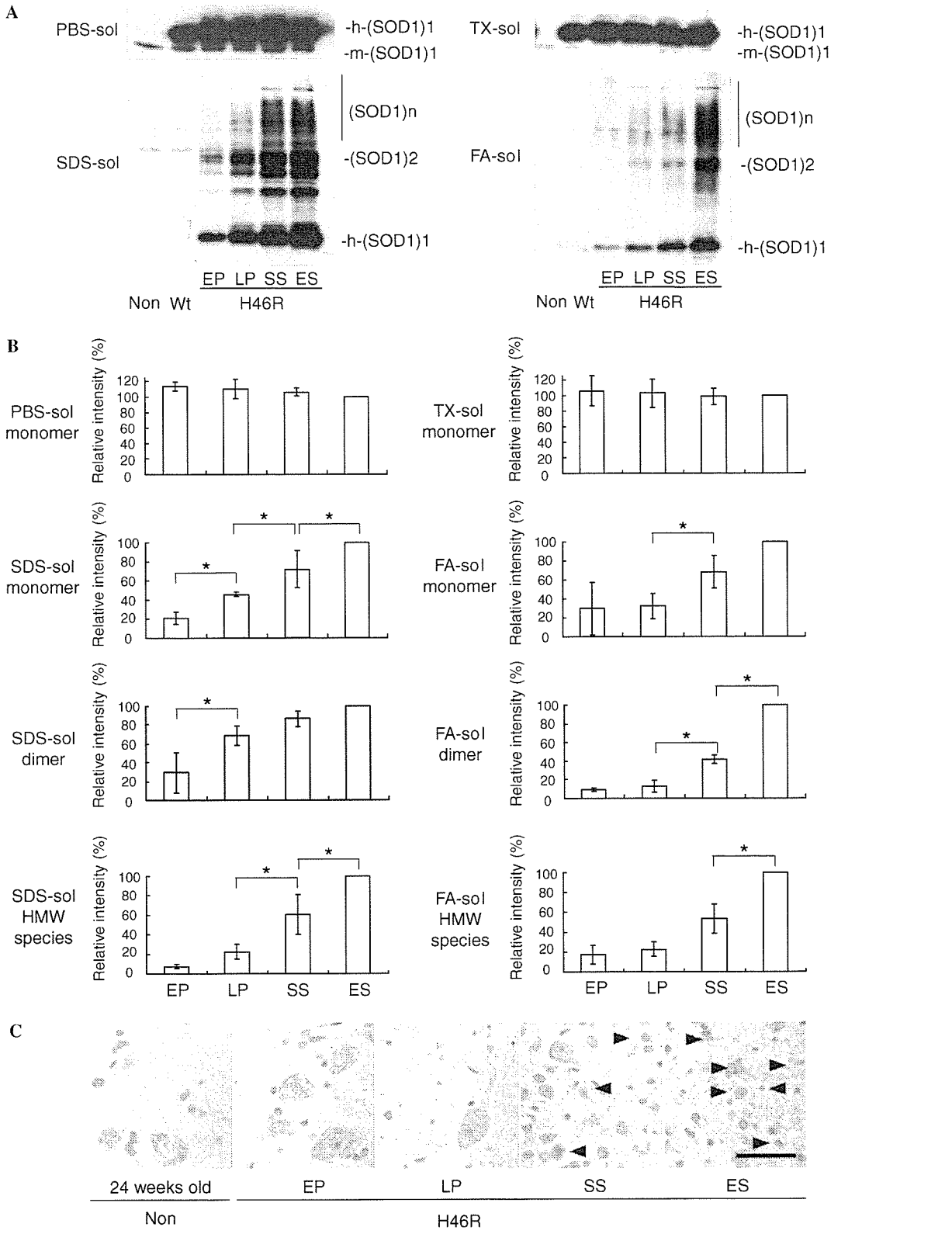

Fig. 2. Age-dependent alteration of SOD1 in spinal cords from H46R SOD1 transgenic mice. (A) The spinal cords of 24-week-old non-transgenic littermates (Non), 38-week-old wild-type SOD1 transgenic mice (Wt), and H46R SOD1 transgenic mice (H46R) at early presymptomatic stage (EP), late presymptomatic stage (LP), symptomatic stage (SS), and end stage (ES) were sequentially fractionated. Ten micrograms of protein from each of the PBS-soluble fraction (PBS-sol), the TX-soluble fraction (TX-sol), and the SDS-soluble fraction (SDS-sol), and equal aliquots of the FA-soluble fraction (FA-sol) were loaded on the gel and then immunoblotted with SOD1-100 antibody. (B) The graphs represent relative intensities of H46R SOD1 species at each stage ($n = 3$, bars represent mean ± SD,* $P < 0.05$). (C) Immunohistochemical analysis of lumbar spinal cords (L_{4-5}) of 24-week-old non-transgenic littermates (Non) and H46R SOD1 transgenic mice (H46R) at four stages. These sections were immunostained with monoclonal anti-SOD1 antibody specific to human SOD1. Scale bars = 50 μm. Arrowheads indicate SOD1-immunoreactive structures.

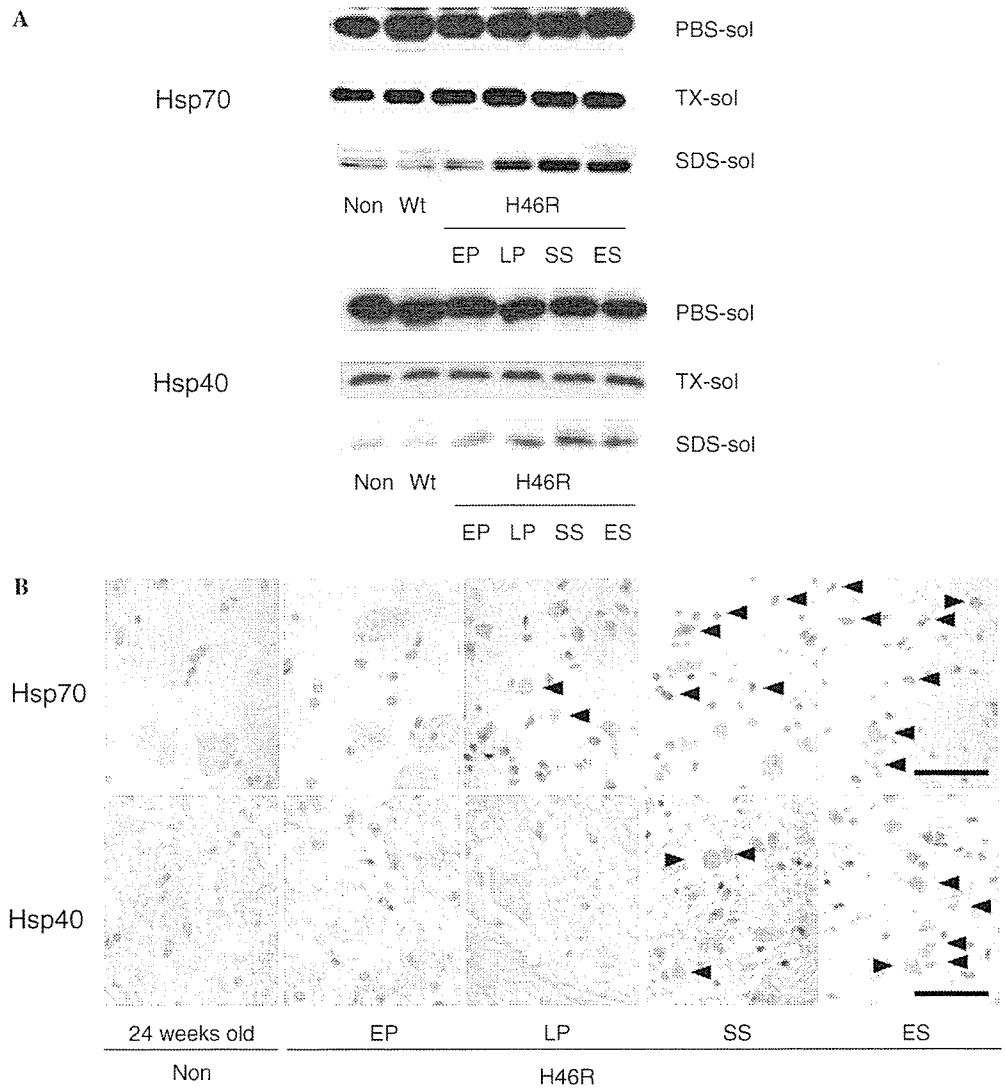

Fig. 3. (A) Increase of Hsp70 and Hsp40 in the SDS-soluble fraction from H46R SOD1 transgenic mice. The fractionated samples used in Fig. 2 were analyzed by Western blotting using anti-Hsp70 and anti-Hsp40 antibodies. Ten micrograms of total protein from each fraction was loaded on each lane. (B) Time course analysis of Hsp-immunoreactive structures. These sections were immunostained with anti-Hsp70 antibody and anti-Hsp40 antibody. Scale bars = 50 μm. Arrowheads indicate immunoreactive structures of each antibody.

the serial sections (data not shown). Although a small number of Hsp70-positive structures were found in neuropil at LP, the increase of SOD1-inclusions containing Hsp70 immunoreactivities was remarkable after SS (Fig. 3B). Similarly, Hsp40-positive structures increased from SS (Fig. 3B). The present data showed that the increase of Hsp70 and Hsp40 in the SDS-soluble fraction appeared along with the increase of SDS-dissociable soluble SOD1 monomers and SDS-stable soluble dimers. This increase of Hsp70 and Hsp40 occurred before the accumulation of visible inclusions with Hsp70 and Hsp40 immunoreactivities.

Inhibition of the proteasome activity promotes the change of SOD1 solubility in cells expressing H46R SOD1

The fALS-linked mutant misfolded SOD1 protein is reported to be degraded by the proteasome pathway [16,17,19,20]. To see how inhibition of the proteasome pathway influences mutant SOD1 solubility, we examined COS-7 cells transiently overexpressing either wild-type SOD1-FLAG or H46R SOD1-FLAG in the presence or absence of proteasome inhibitor MG132. In this experiment, FLAG-tagged SOD1 was used for discriminating exogenous SOD1 from endogenous SOD1 by migrating more slowly. Collected cell pellets were sequentially extracted with PBS, 1% TX, and 5% SDS. In the PBS-soluble and the TX-soluble fractions, the levels of mutant SOD1 as well as wild-type SOD1 slightly increased when MG132 was added in a dose-dependent manner (Fig. 4A). In the SDS-soluble fraction, a small amount of wild-type monomeric SOD1 was seen in the absence of MG132. The levels of wild-type SOD1 monomers increased without generating HMW species in the presence of 10 μM MG132. On the other hand, in the SDS-soluble fraction, mutant SOD1 monomers and dimers were obviously

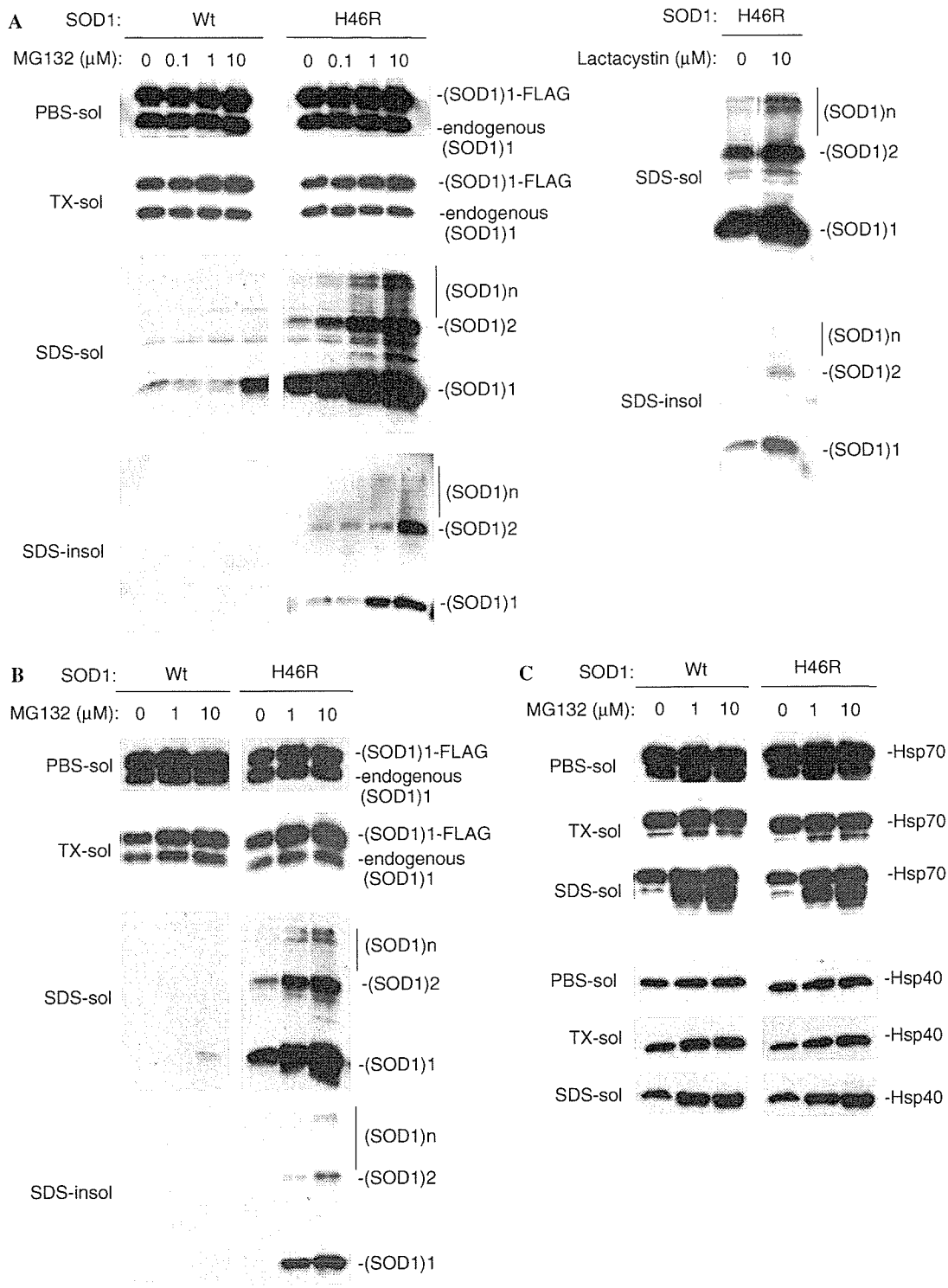

Fig. 4. Alteration of H46R SOD1 solubility in COS-7 and SH-SY5Y cells by treatment with proteasome inhibitors. COS-7 cells (A) and SH-SY5Y cells (B,C) were transiently transfected with either wild-type SOD1-FLAG pcDNA3.1 or H46R SOD1-FLAG pcDNA3.1. At 24 h after transfection, the culture medium was replaced with a fresh one containing the indicated concentrations of proteasome inhibitor, either MG132 (left panels of (A) and all panels of (B)) or lactacystin (right panels of (A)). Cells were incubated for an additional 24 h. Collected cell pellets were serially fractionated to the PBS-soluble fraction (PBS-sol), the TX-soluble fraction (TX-sol), the SDS-soluble fraction (SDS-sol), and the SDS-insoluble fraction (SDS-insol). Ten micrograms of protein from each of the PBS-soluble fraction, the TX-soluble fraction, and the SDS-soluble fraction, and equal aliquots of the SDS-insoluble fraction were subjected to the gel and immunoblotted with SOD1-100 (A,B). (C) The levels of both endogenous Hsp70 and Hsp40 were elevated in the SDS-soluble fraction from cells expressing wild-type SOD1 as well as mutant SOD1 in an MG-132 dose-dependent manner. The fractionated samples used in (B) were analyzed by Western blotting using anti-Hsp70 and anti-Hsp40 antibodies.

detected in the absence of MG132 and showed a significant increase in generating HMW species by treatment with MG132 in a dose-dependent manner (Fig. 4A). Similarly, in the SDS-insoluble fraction, the levels of mutant SOD1 monomers, dimers, and HMW species elevated by treatment with MG132 in a dose-dependent manner, while wild-type SOD1 was not detected (Fig. 4A). Dose-dependent treatment with MG132 further showed that the elevation of SDS-dissociable soluble mutant SOD1 monomers and SDS-stable soluble dimers preceded that of SDS-stable soluble HMW species and SDS-insoluble species. Treatment with another specific proteasome inhibitor, lactacystin, also caused the accumulation of SDS-soluble and SDS-insoluble mutant SOD1 species in COS-7 cells, although to a lesser extent (Fig. 4A). We further confirmed the effect of MG132 on the alteration of SOD1 solubility in human neuroblastoma SH-SY5Y cells. By treatment with MG132, SDS-soluble and SDS-insoluble mutant SOD1 monomers, dimers, and HMW species accumulated in mutant-specific and dose-dependent manners in SH-SY5Y cells similar to COS-7 cells (Fig. 4B). The elevation of SDS-dissociable soluble mutant SOD1 monomers and SDS-stable soluble dimers also preceded that of SDS-stable soluble HMW species and SDS-insoluble species. In SH-SY5Y cells expressing mutant SOD1, the levels of both endogenous Hsp70 and Hsp40 were elevated in the SDS-soluble fraction in an MG-132 dose-dependent manner (Fig. 4C). However, the increase of endogenous Hsp70 and Hsp40 levels in the SDS-soluble fraction was similarly observed in cells expressing wild-type SOD1 (Fig. 4C). These results showed that inhibition of the proteasome activity in mutant SOD1 expressed cells recapitulated the alteration of SOD1 solubility with aging in mutant transgenic mice. Inhibition of the proteasome activity initially led to the accumulation of SDS-dissociable soluble mutant SOD1 monomers and SDS-stable soluble dimers prior to that of SDS-stable soluble HMW species and SDS-insoluble species irrespective of the increase of endogenous Hsp70 and Hsp40.

Effect of overexpression of Hsp70 on the accumulation of SDS-soluble and SDS-insoluble mutant SOD1 species

Overexpression of Hsp70 has been reported to reduce the SOD1-aggregate formation and prolong cellular viability in a cellular model of fALS [23]. As described in our previous report [20], overexpression of mutant SOD1 pEF-BOS in COS-7 cells causes higher expression levels of SOD1 than overexpression of mutant SOD1 pcDNA3.1, and a large amount of SDS-insoluble mutant SOD1 appears without adding proteasome inhibitor. By taking advantage of this high-expression system, we investigated cells co-transfected with mutant H46R SOD1 cDNA and a 4-fold molar excess of Hsp cDNA to see the effect of Hsp70 and Hsp40 on the levels of altered insoluble SOD1 species (Fig. 5A). Overexpression of Hsp70 obviously reduced the levels of SDS-dissociable soluble mutant SOD1 monomers, SDS-stable soluble dimers, and SDS-stable soluble HMW species, compared to co-expression of the empty vector (Fig. 5A). Overexpression of Hsp40 showed a weaker effect on the levels of SDS-soluble mutant SOD1 species (Fig. 5A). Co-overexpression with Hsp70 plus Hsp40 enhanced the effect of Hsp70 on a decrease of the levels of SDS-stable soluble mutant SOD1 dimers and HMW species (Fig. 5A). In the SDS-insoluble fraction, overexpression of Hsp70 also led to a reduction in the levels of SDS-dissociable insoluble mutant SOD1 monomers, SDS-stable insoluble dimers, and SDS-stable insoluble HMW species, and the effect was enhanced by co-overexpression of Hsp40 (Fig. 5A). This finding was also observed in cells expressing different fALS-linked mutant G93A SOD1 (data not shown). To further examine the molecular mechanism by which overexpression of Hsp70 reduced insoluble mutant SOD1 species, cells were co-transfected with H46R SOD1 and Hsp70 cDNAs in various molar ratios (Fig. 5B). The levels of mutant SOD1 monomers, dimers, and HMW species in the SDS-soluble fraction as well as in the SDS-insoluble fraction decreased in negative correlation to the amounts of transfected Hsp70 cDNA (Figs. 5B and C). On the other hand, the levels of mutant SOD1 monomers in the PBS-soluble and TX-soluble fractions did not increase, in sharp contrast to the significant reduction of the amount of SDS-soluble species by overexpression of Hsp70 (Figs. 5B and C). These findings demonstrated that overexpressed Hsp70 modulated the levels at SDS-dissociable soluble mutant SOD1 monomers and SDS-stable soluble dimers as misfolded proteins and preferentially forwarded abnormally insoluble SOD1 species to degradation rather than to refolding.

Discussion

Although wild-type SOD1 is principally a soluble, cytosolic protein [4], fALS-linked mutant SOD1 has a tendency to assemble as insoluble aggregates, which are immunohistochemically observed as cytoplasmic inclusions in patients with fALS having SOD1 mutation [10]. There has been controversy about whether such inclusions are a cause or simply a result of the neuronal degeneration. Immunohistochemical experiments do not rule out the possibility that mutant SOD1 aggregates can damage motor neurons, even though microscopically visible inclusions are absent in the early period. In agreement with the previous finding [16,19], our immunohistochemical data demonstrated that SOD1-positive inclusions appeared after disease onset, and the accumulation of SOD1-positive inclusions was parallel to the elevation of most insoluble SOD1 species recovered in the FA-soluble fraction. On the other hand, we revealed that mutant H46R SOD1 began to significantly alter its solubility to SDS-dissociable soluble monomers and SDS-stable soluble dimers earlier than the appearance of visible SOD1-positive inclusions. These findings suggest that complexes of SDS-dissociable soluble SOD1 monomers and SDS-stable soluble dimers were much smaller in

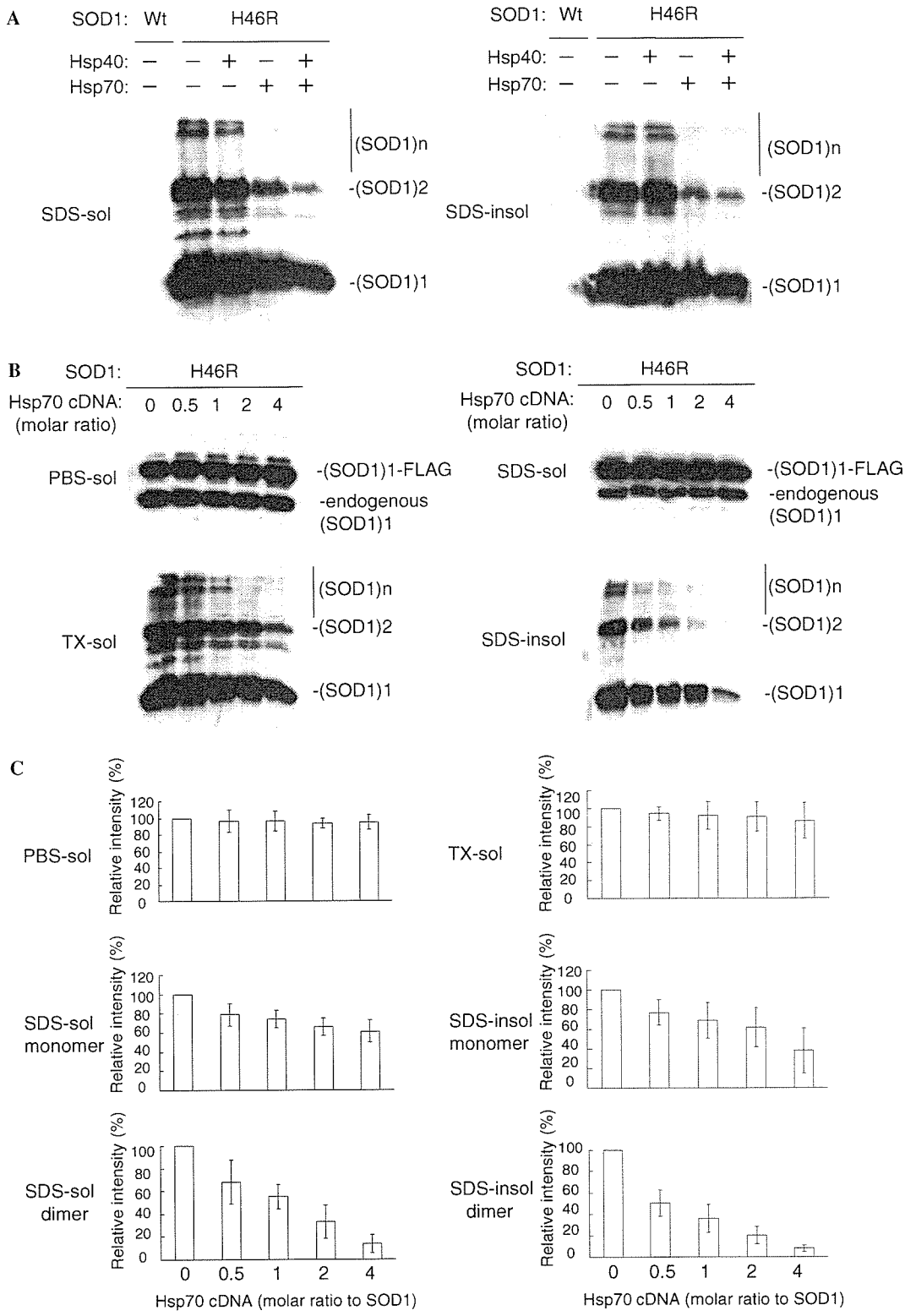

Fig. 5. The effect of overexpression of Hsp70 and Hsp40 on the level of altered insoluble mutant SOD1 in intact cells. (A) Western blots of COS-7 cells co-transfected with H46R SOD1-FLAG pEF-BOS and either pCMV-Hsp70 or pRC-Hsp40 (molar ratio of Hsp versus SOD1 cDNA was 4:1) using SOD1-100 antibody. Proteins from the SDS-soluble (SDS-sol) and SDS-insoluble (SDS-insol) fractions were loaded to the gel and immunoblotted with SOD1-100 antibody. (B) Western blot analysis of cells co-transfected with H46R SOD1-FLAG pEF-BOS and various amounts of Hsp70 cDNA. Molar ratios of pCMV-Hsp70 versus H46R SOD1-FLAG pEF-BOS are indicated in the figure. Forty-eight hours after transfection, cells were harvested and fractionated. Proteins from each fraction were analyzed by Western blotting using an SOD1-100 antibody. (C) The graphs show the relative intensities of H46R SOD1 monomers and dimers in each fraction shown in (B). The relative intensities were quantified by densitometry and normalized to bands from cells transfected with the empty vector ($n = 3$, bars represent mean ± SD).

size than visible inclusions, and the presence of visible inclusions composed of highly insoluble aggregates contributes less to the early pathological event.

Our findings are relevant to the previous reports that detergent-insoluble dimers and HMW species were found before onset of motor disability and the appearance of pathological SOD1-aggregates in mutant SOD1 transgenic mice [16,19]. However, in these preceding experiments, the alteration of mutant SOD1 solubility was assessed by fractionation using only one detergent. By the sequential extraction of mutant transgenic mouse spinal cords with PBS and TX containing buffer for removing cytosolic and mitochondrial SOD1 with normal solubility equivalent to wild-type SOD1, we separated H46R SOD1 into three different kinds of mutant-specific insoluble species, indicating that insoluble mutant SOD1 did not consist of a uniform species. To see whether SDS-dissociable soluble monomers, in addition to SDS-stable soluble dimers, represented early misfolded intermediates, we have investigated the alteration of SOD1 solubility using a cell culture model of fALS. Treatment with proteasome inhibitors caused the accumulation of SDS-dissociable soluble mutant H46R SOD1 monomers and SDS-stable soluble dimers earlier than that of SDS-stable soluble HMW species and SDS-insoluble species. This finding resembled the age-dependent alteration of SOD1 solubility in mutant H46R SOD1 transgenic mice. In contrast, overexpression of Hsp70 reduced the levels of SDS-dissociable soluble mutant H46R SOD1 monomers and SDS-stable soluble dimers. These findings indicate that SDS-dissociable soluble mutant SOD1 monomers and SDS-stable soluble dimers are degraded by the proteasome pathway and are modulated by molecular chaperones as misfolded intermediates. The previous in vitro study showed that a normal homodimer of SOD1 dissociates to an aggregation-prone monomeric intermediate by oxidation [32]. Further experiments would be necessary to see how potentially aggregation-promoting modifications, such as oxidation and nitration, relate to the alteration of SOD1 solubility.

Several reports showed that Hsp70 and its co-chaperone Hsp40 were involved in the aggregation process or the degradation of SOD1 [11,33], and Hsp70 and Hsp40 suppress SOD1 aggregate formation and improve neurite outgrowth [34]. Although in the previous report up-regulation of Hsp70 was not observed in the spinal cords of mutant SOD1 transgenic mice in contrast to cultured cells overexpressing mutant SOD1 [23], we found that the levels of Hsp70 and Hsp40 in mutant SOD1 transgenic mice increased in the SDS-soluble fraction before disease onset. This observation is consistent with the report that Hsp70 interacts with detergent-insoluble SOD1 rather than detergent-soluble SOD1 in cells [33]. However, it should be noted that endogenous Hsp70 and Hsp40 in the SDS-soluble fraction do not suppress accumulation of insoluble mutant SOD1 in the present H46R SOD1 transgenic mice. Furthermore, Liu et al. [35] showed that elevation of Hsp70 does not affect ALS disease onset and survival in several types of mutant SOD1 transgenic mice co-overexpressing Hsp70 at ~10-fold higher levels than control mice, suggesting that there was no benefit from chronically elevated Hsp70. In cells, overexpression of Hsp70 reduced the levels of SDS-soluble and SDS-insoluble mutant H46R SOD1, whereas it did not lead to the elevation of PBS-soluble and TX-soluble SOD1 levels. This result implies that overexpression of Hsp70 had an effect on the levels of mutant-specific insoluble SOD1 species by forwarding them to the degradation pathway rather than refolding them to a normal soluble pool of SOD1. Adachi et al. [36] reported that overexpression of Hsp70 decreased soluble monomeric androgen receptor (AR) protein in addition to HMW mutant AR protein in double transgenic mice expressing mutant AR protein and Hsp70, suggesting that Hsp70 enhanced mutant AR degradation. Since inhibition of the proteasome activity in cells had a strong effect on the accumulation of insoluble mutant SOD1 with up-regulation of endogenous Hsp70 and Hsp40, the discrepancy in beneficial effects of Hsp70 between cellular and mouse models of fALS may be explained by several possibilities. First, the diminishing of the proteasome activity may generate abundant misfolded proteins whose concentration exceeds the capacity of up-regulated endogenous Hsp70/40. Second, the main function of Hsp70 is to facilitate the proteasome pathway-dependent clearance of misfolded SOD1. Third, the accumulation of insoluble SOD1 species directly impairs the chaperone function of Hsp70 [37]. An approach for examining the toxicity of SDS-dissociable soluble mutant SOD1 monomers and SDS-stable soluble dimers may provide a clue to prevent a further accumulation of potentially toxic misfolded protein complexes in fALS.

Acknowledgments

This work was supported by Research Grants from the Japan ALS association (S.A.), a Grant-in-Aid for Scientific Research on Priority Areas (Advanced Brain Science Project) from the Ministry of Education, Culture, Sports, Science and Technology, Japan (S.A.), and a Research Grant on Measures for Intractable Diseases from the Ministry of Health, Labour and Welfare (T.K.).

References

[1] D.R. Rosen, T. Siddique, D. Patterson, D.A. Figlewicz, P. Sapp, A. Hentati, D. Donaldson, J. Goto, J.P. O'Regan, H.X. Deng, et al., Mutations in Cu/Zn superoxide dismutase gene are associated with familial amyotrophic lateral sclerosis, Nature 362 (1993) 59–62.

[2] M.E. Cudkowicz, D. McKenna-Yasek, P.E. Sapp, W. Chin, B. Geller, D.L. Hayden, D.A. Schoenfeld, B.A. Hosler, H.R. Horvitz, R.H. Brown, Epidemiology of mutations in superoxide dismutase in amyotrophic lateral sclerosis, Ann. Neurol. 41 (1997) 210–221.

[3] J.S. Valentine, P.J. Hart, Misfolded CuZnSOD and amyotrophic lateral sclerosis, Proc. Natl. Acad. Sci. USA 100 (2003) 3617–3622.

[4] A. Okado-Matsumoto, I. Fridovich, Subcellular distribution of superoxide dismutases (SOD) in rat liver: Cu,Zn-SOD in mitochondria, J. Biol. Chem. 276 (2001) 38388–38393.

[5] A.G. Reaume, J.L. Elliott, E.K. Hoffman, N.W. Kowall, R.J. Ferrante, D.F. Siwek, H.M. Wilcox, D.G. Flood, M.F. Beal, R.H. Brown Jr., R.W. Scott, W.D. Snider, Motor neurons in Cu/Zn superoxide dismutase-deficient mice develop normally but exhibit enhanced cell death after axonal injury, Nat. Genet. 13 (1996) 43–47.

[6] M.E. Gurney, H. Pu, A.Y. Chiu, M.C. Dal Canto, C.Y. Polchow, D.D. Alexander, J. Caliendo, A. Hentati, Y.W. Kwon, H.X. Deng, et al., Motor neuron degeneration in mice that express a human Cu,Zn superoxide dismutase mutation, Science 264 (1994) 1772–1775.

[7] M.E. Ripps, G.W. Huntley, P.R. Hof, J.H. Morrison, J.W. Gordon, Transgenic mice expressing an altered murine superoxide dismutase gene provide an animal model of amyotrophic lateral sclerosis, Proc. Natl. Acad. Sci. USA 92 (1995) 689–693.

[8] P.C. Wong, C.A. Pardo, D.R. Borchelt, M.K. Lee, N.G. Copeland, N.A. Jenkins, S.S. Sisodia, D.W. Cleveland, D.L. Price, An adverse property of a familial ALS-linked SOD1 mutation causes motor neuron disease characterized by vacuolar degeneration of mitochondria, Neuron 14 (1995) 1105–1116.

[9] L.I. Bruijn, M.W. Becher, M.K. Lee, K.L. Anderson, N.A. Jenkins, N.G. Copeland, S.S. Sisodia, J.D. Rothstein, D.R. Borchelt, D.L. Price, D.W. Cleveland, ALS-linked SOD1 mutant G85R mediates damage to astrocytes and promotes rapidly progressive disease with SOD1-containing inclusions, Neuron 18 (1997) 327–338.

[10] N. Shibata, A. Hirano, M. Kobayashi, T. Siddique, H.X. Deng, W.Y. Hung, T. Kato, K. Asayama, Intense superoxide dismutase-1 immunoreactivity in intracytoplasmic hyaline inclusions of familial amyotrophic lateral sclerosis with posterior column involvement, J. Neuropathol. Exp. Neurol. 55 (1996) 481–490.

[11] M. Watanabe, M. Dykes-Hoberg, V.C. Culotta, D.L. Price, P.C. Wong, J.D. Rothstein, Histological evidence of protein aggregation in mutant SOD1 transgenic mice and in amyotrophic lateral sclerosis neural tissues, Neurobiol. Dis. 8 (2001) 933–941.

[12] P.A. Jonsson, K. Ernhill, P.M. Andersen, D. Bergemalm, T. Brannstrom, O. Gredal, P. Nilsson, S.L. Marklund, Minute quantities of misfolded mutant superoxide dismutase-1 cause amyotrophic lateral sclerosis, Brain 127 (2004) 73–88.

[13] H.D. Durham, J. Roy, L. Dong, D.A. Figlewicz, Aggregation of mutant Cu/Zn superoxide dismutase proteins in a culture model of ALS, J. Neuropathol. Exp. Neurol. 56 (1997) 523–530.

[14] T. Koide, S. Igarashi, K. Kikugawa, R. Nakano, T. Inuzuka, M. Yamada, H. Takahashi, S. Tsuji, Formation of granular cytoplasmic aggregates in COS7 cells expressing mutant Cu/Zn superoxide dismutase associated with familial amyotrophic lateral sclerosis, Neurosci. Lett. 257 (1998) 29–32.

[15] M. Nagai, M. Aoki, I. Miyoshi, M. Kato, P. Pasinelli, N. Kasai, R.H. Brown Jr., Y. Itoyama, Rats expressing human cytosolic copper-zinc superoxide dismutase transgenes with amyotrophic lateral sclerosis: associated mutations develop motor neuron disease, J. Neurosci. 21 (2001) 9246–9254.

[16] J.A. Johnston, M.J. Dalton, M.E. Gurney, R.R. Kopito, Formation of high molecular weight complexes of mutant Cu, Zn-superoxide dismutase in a mouse model for familial amyotrophic lateral sclerosis, Proc. Natl. Acad. Sci. USA 97 (2000) 12571–12576.

[17] K. Puttaparthi, C. Wojcik, B. Rajendran, G.N. DeMartino, J.L. Elliott, Aggregate formation in the spinal cord of mutant SOD1 transgenic mice is reversible and mediated by proteasomes, J. Neurochem. 87 (2003) 851–860.

[18] J. Wang, G. Xu, D.R. Borchelt, High molecular weight complexes of mutant superoxide dismutase 1: age-dependent and tissue-specific accumulation, Neurobiol. Dis. 9 (2002) 139–148.

[19] M. Urushitani, J. Kurisu, K. Tsukita, R. Takahashi, Proteasomal inhibition by misfolded mutant superoxide dismutase 1 induces selective motor neuron death in familial amyotrophic lateral sclerosis, J. Neurochem. 83 (2002) 1030–1042.

[20] S. Tobisawa, Y. Hozumi, S. Arawaka, S. Koyama, M. Wada, M. Nagai, M. Aoki, Y. Itoyama, K. Goto, T. Kato, Mutant SOD1 linked to familial amyotrophic lateral sclerosis, but not wild-type SOD1, induces ER stress in COS7 cells and transgenic mice, Biochem. Biophys. Res. Commun. 303 (2003) 496–503.

[21] D.H. Hyun, M. Lee, B. Halliwell, P. Jenner, Proteasomal inhibition causes the formation of protein aggregates containing a wide range of proteins, including nitrated proteins, J. Neurochem. 86 (2003) 363–373.

[22] E. Kabashi, J.N. Agar, D.M. Taylor, S. Minotti, H.D. Durham, Focal dysfunction of the proteasome: a pathogenic factor in a mouse model of amyotrophic lateral sclerosis, J. Neurochem. 89 (2004) 1325–1335.

[23] W. Bruening, J. Roy, B. Giasson, D.A. Figlewicz, W.E. Mushynski, H.D. Durham, Up-regulation of protein chaperones preserves viability of cells expressing toxic Cu/Zn-superoxide dismutase mutants associated with amyotrophic lateral sclerosis, J. Neurochem. 72 (1999) 693–699.

[24] C.A. Ross, M.A. Poirier, Protein aggregation and neurodegenerative disease, Nat. Med. 10 (Suppl.) (2004) S10–S17.

[25] A.A. Michels, B. Kanon, A.W. Konings, K. Ohtsuka, O. Bensaude, H.H. Kampinga, Hsp70 and Hsp40 chaperone activities in the cytoplasm and the nucleus of mammalian cells, J. Biol. Chem. 272 (1997) 33283–33289.

[26] Y. Kobayashi, A. Kume, M. Li, M. Doyu, M. Hata, K. Ohtsuka, G. Sobue, Chaperones Hsp70 and Hsp40 suppress aggregate formation and apoptosis in cultured neuronal cells expressing truncated androgen receptor protein with expanded polyglutamine tract, J. Biol. Chem. 275 (2000) 8772–8778.

[27] S. Arawaka, H. Hasegawa, A. Tandon, C. Janus, F. Chen, G. Yu, K. Kikuchi, S. Koyama, T. Kato, P.E. Fraser, P. St. George-Hyslop, The levels of mature glycosylated nicastrin are regulated and correlate with gamma-secretase processing of amyloid beta-precursor protein, J. Neurochem. 83 (2002) 1065–1071.

[28] R. Chang-Hong, M. Wada, S. Koyama, H. Kimura, S. Arawaka, T. Kawanami, K. Kurita, T. Kadoya, M. Aoki, Y. Itoyama, T. Kato, Neuroprotective effect of oxidized galectin-1 in a transgenic mouse model of amyotrophic lateral sclerosis, Exp. Neurol. 194 (2005) 203–211.

[29] C.J. Epstein, K.B. Avraham, M. Lovett, S. Smith, O. Elroy-Stein, G. Rotman, C. Bry, Y. Groner, Transgenic mice with increased Cu/Zn-superoxide dismutase activity: animal model of dosage effects in Down syndrome, Proc. Natl. Acad. Sci. USA 84 (1987) 8044–8048.

[30] H. Fujiwara, M. Hasegawa, N. Dohmae, A. Kawashima, E. Masliah, M.S. Goldberg, J. Shen, K. Takio, T. Iwatsubo, alpha-Synuclein is phosphorylated in synucleinopathy lesions, Nat. Cell. Biol. 4 (2002) 160–164.

[31] P.J. Kahle, M. Neumann, L. Ozmen, V. Muller, S. Odoy, N. Okamoto, H. Jacobsen, T. Iwatsubo, J.Q. Trojanowski, H. Takahashi, K. Wakabayashi, N. Bogdanovic, P. Riederer, H.A. Kretzschmar, C. Haass, Selective insolubility of alpha-synuclein in human Lewy body diseases is recapitulated in a transgenic mouse model, Am. J. Pathol. 159 (2001) 2215–2225.

[32] R. Rakhit, J.P. Crow, J.R. Lepock, L.H. Kondejewski, N.R. Cashman, A. Chakrabartty, Monomeric Cu,Zn-superoxide dismutase is a common misfolding intermediate in the oxidation models of sporadic and familial amyotrophic lateral sclerosis, J. Biol. Chem. 279 (2004) 15499–15504.

[33] G.A. Shinder, M.C. Lacourse, S. Minotti, H.D. Durham, Mutant Cu/Zn-superoxide dismutase proteins have altered solubility and interact with heat shock/stress proteins in models of amyotrophic lateral sclerosis, J. Biol. Chem. 276 (2001) 12791–12796.

[34] H. Takeuchi, Y. Kobayashi, T. Yoshihara, J. Niwa, M. Doyu, K. Ohtsuka, G. Sobue, Hsp70 and Hsp40 improve neurite outgrowth and suppress intracytoplasmic aggregate formation in cultured neuronal cells expressing mutant SOD1, Brain Res. 949 (2002) 11–22.

[35] J. Liu, L.A. Shinobu, C.M. Ward, D. Young, D.W. Cleveland, Elevation of the Hsp70 chaperone does not effect toxicity in mouse

models of familial amyotrophic lateral sclerosis, J. Neurochem. 93 (2005) 875–882.
[36] H. Adachi, M. Katsuno, M. Minamiyama, C. Sang, G. Pagoulatos, C. Angelidis, M. Kusakabe, A. Yoshiki, Y. Kobayashi, M. Doyu, G. Sobue, Heat shock protein 70 chaperone overexpression ameliorates phenotypes of the spinal and bulbar muscular atrophy transgenic mouse model by reducing nuclear-localized mutant androgen receptor protein, J. Neurosci. 23 (2003) 2203–2211.
[37] H. Tummala, C. Jung, A. Tiwari, C.M. Higgins, L.J. Hayward, Z. Xu, Inhibition of chaperone activity is a shared property of several Cu,Zn-superoxide dismutase mutants that cause amyotrophic lateral sclerosis, J. Biol. Chem. 280 (2005) 17725–17731.

WILEY InterScience
Journal of Neuroscience Research 85:395–401 (2007)

Role of p53 in Neurotoxicity Induced by the Endoplasmic Reticulum Stress Agent Tunicamycin in Organotypic Slice Cultures of Rat Spinal Cord

Jun Tashiro,[1]* Seiji Kikuchi,[1] Kazuyoshi Shinpo,[2] Riichiro Kishimoto,[1] Sachiko Tsuji,[1] and Hidenao Sasaki[1]

[1]Department of Neurology, Hokkaido University Graduate School of Medicine, Kita-ku, Sapporo, Hokkaido, Japan
[2]Nishimaruyama Hospital, Chuo-ku, Sapporo, Hokkaido, Japan

The endoplasmic reticulum (ER) is important for maintaining the quality of cellular proteins. Various stimuli can disrupt ER homeostasis and cause the accumulation of unfolded or misfolded proteins, i.e., a state of ER stress. Recently, ER stress has been reported to play an important role in the pathogenesis of neurological disorders such as cerebral ischemia and neurodegenerative diseases, but its involvement in the spinal cord diseases has not been fully discussed. We conducted this study using tunicamycin (Tm) as an ER stress inducer for rat spinal cord in organotypic slice culture, a system that we have recently established. Tm was shown to induce ER stress by increased expression of GRP78. The viability rate of spinal cord neurons decreased in a dose-dependent manner with Tm treatment, and dorsal horn interneurons were more vulnerable to Tm-induced neurotoxicity. A p53 inhibitor significantly increased the viability of dorsal horn interneurons, and immunofluorescence studies showed nuclear accumulation of p53 in the dorsal horns of Tm-treated spinal cord slices. These findings suggest that p53 plays an important role in the killing of dorsal horn interneurons by Tm. In contrast, motor neurons were not protected by the p53 inhibitor, suggesting that the role of p53 may vary between different cell types. This difference might be a clue to the mechanism of the stress-response pathway and might also contribute to the potential application of p53 inhibitors for the treatment of spinal cord diseases, including amyotrophic lateral sclerosis.

Key words: endoplasmic reticulum; unfolded protein response; dorsal horn interneuron; pifithrin-α

The endoplasmic reticulum (ER) is an intracellular organelle that is important for the folding and maturation of transmembrane and secretory proteins (Liu and Kaufman, 2003). The ER is highly sensitive to alterations of cellular homeostasis and provides strict quality control to ensure that only correctly folded proteins are transported to the Golgi apparatus. A number of biochemical and physiologic stimuli can disrupt ER homeostasis and cause the intraluminal accumulation of unfolded or misfolded proteins, when cells activate a signaling pathway called *unfolded protein response* (UPR; Zhang and Kaufman, 2006). The UPR includes induction of the transcription of UPR genes, a translational attenuation of global protein synthesis, and ER-associated degradation (Liu and Kaufman, 2003). If cells fail to cope with the adverse stimuli by these responses, apoptosis is inevitable.

Recently, ER stress has been reported to play an important role in the pathogenesis of a wide variety of neurological conditions (Shen et al., 2004; Paschen and Mengesdorf, 2005), such as cerebral ischemia (DeGracia and Montie, 2004), and neurodegenerative diseases, including Alzheimer's disease (Katayama et al., 2004) and Parkinson's disease (Paschen and Frandsen, 2001; Takahashi et al., 2003; Takahashi and Imai, 2003; Kheradpezhouh et al., 2003), and polyglutamine diseases (Nishitoh et al., 2002) as well as prion diseases (Hetz et al., 2003), Pelizaeus-Merzbacher disease (Swanton et al., 2005), GM1 gangliosidosis (Tessitore et al., 2004), and inclusion body myositis (Vattemi et al., 2004). However, most experiments reported so far have involved cell lines, and only a few studies have used spinal cord cells to assess the pathogenesis of spinal cord disease

Contract grant sponsor: Research Committee for CNS Degenerative Disease and Group Research in the Pathogenesis and Pathomechanism of Amyotrophic Lateral Sclerosis, Ministry of Health, Labor and Welfare of Japan.

*Correspondence to: Jun Tashiro, Department of Neurology, Hokkaido University Graduate School of Medicine, Kita-15 Nishi-7 Kita-ku, Sapporo, Hokkaido, 060-8638 Japan. E-mail: jtashiro@med.hokudai.ac.jp

Received 19 April 2006; Revised 18 August 2006; Accepted 16 September 2006

Published online 27 November 2006 in Wiley InterScience (www.interscience.wiley.com). DOI: 10.1002/jnr.21120

from the perspective of ER stress (Tobisawa et al., 2003; Wootz et al., 2004).

Amyotrophic lateral sclerosis (ALS) is a neurodegenerative disease that selectively affects the upper and lower motor neurons. Most ALS cases are sporadic, but approximately 10% are familial. Among the familial patients, about 20% have mutations of the gene encoding Cu/Zn superoxide dismutase (SOD1; Rosen et al., 1993; Hervias et al., 2005). Mutations of the SOD1 gene and the associated mechanisms leading to neuronal death such as mitochondrial dysfunction (Hervias et al., 2005), fragmentation of the Golgi apparatus (Fujita and Okamoto, 2005), and activation of caspases (Wootz et al., 2004) have been discussed extensively, but the contribution of ER stress has not yet been fully elucidated (Tobisawa et al., 2003).

We have been investigating the mechanisms of neuronal damage in the spinal cord. Our previous studies were focused on dysfunction of the ubiquitin-proteasome system (Kikuchi et al., 2002), ER stress (Kikuchi et al., 2003), and the related effector pathways. In these two studies, we used lactacystin and epoxomicin as proteasome inhibitors and brefeldin A (BFA) as the ER stress inducer, in a dissociated culture system, and the results of both studies suggested that motor neurons were more vulnerable to the toxicity of those agents than nonmotor neurons.

More recently, we established an organotypic slice culture method for rat spinal cord that makes it easier to identify each cell type accurately, because the architecture of the spinal cord is preserved in the transverse plane (Tsuji et al., 2005). By using this method, we evaluated the effect of proteasome inhibition on rat spinal cord neurons, and selective toxicity for motor neurons was clearly demonstrated. To evaluate further the effects of ER stress on spinal cord neurons, we conducted the present study with another ER stress inducer, tunicamycin (Tm), and the organotypic slice culture system. In addition, studies with p53 inhibitor were performed to investigate the role of p53 in the pathways leading to neuronal death.

MATERIALS AND METHODS

All procedures were performed in accordance with the Guide for the Care and Use of Laboratory Animals, Hokkaido University Graduate School of Medicine.

Materials

The drugs and reagents used in our experiments were as follows: SMI-32 (Sternberger Monoclonals Incorporated, Lutherville, MD), anti-calretinin antibody (Chemicon, Temecula, CA), anti-p53 monoclonal antibody (BD-Biosciences, San Jose, CA), anti-p53 polyclonal antibody (Santa Cruz Biotechnology, Santa Cruz, CA), anti-glucose-regulated protein (GRP) 78 antibody (StressGen Biotechnologies, San Diego, CA), anti-β-actin antibody (Sigma, St. Louis, MO), peroxidase anti-mouse IgG (H + L) and anti-rabbit IgG antibodies (Vector, Burlingame, CA), Alexa Flour 488 goat anti-mouse IgG and Alexa Flour 568 goat anti-rabbit IgG antibodies (Molecular Probes, Eugene, OR), Eagle's minimum essential medium and glutamine (Nissui, Tokyo, Japan), fetal bovine serum and Gey's balanced solution (Sigma), Hank's balanced salt solution (Gibco BRL, Grand Island, NY), brefeldin A and tunicamycin (Sigma); pifithrin-α (Calbiochem, San Diego, CA), and Hoechst 33258 (Sigma).

Organotypic Slice Culture

Organotypic slice cultures were prepared as described previously (Tsuji et al., 2005). Under deep anesthesia with ketamine, neonatal Sprague-Dawley rats on the day 7 were euthanized by decapitation, and their lumbar spinal cords were removed. Nerve roots and excess connective tissue were removed in cooled Gey's balanced salt solution containing 6.5 mg/ml glucose. Then, the spinal cords were cut into 400-μm slices with a McIlwain tissue chopper (Mickle Laboratory Engineering, Gomshall, Surrey, United Kingdom). Four or five slices were set on a membrane insert (Millicell-CM, Millipore, Bedford, MA) and placed into a six-well culture dish with 1 ml of culture medium consisting of 50% Eagle's minimum essential medium, 25% Hank's balanced salt solution, 25% horse serum, 6.4 mg/ml glucose, and 2 mM l-glutamine. The slices were incubated at 37°C in a 5% CO_2 incubator, and the culture medium was changed twice per week. All cultures were used in the experiments after 10 days in vitro.

Experimental Treatment

The spinal cord slices were exposed to Tm at various concentrations (1–20 μg/ml) and BFA at 50 μM on the tenth day of culture. Slices were incubated for about 24 hr before performing Western blot analysis and for about 72 hr before Western blotting and immunohistochemistry or immunofluorescence in a 5% CO_2 incubator maintained at 37°C. To study the protective effect against Tm-induced toxicity, a synthetic inhibitor of p53 [pifithrin-α (PFT)] was added to the culture medium simultaneously with Tm. All reagents added to the culture medium were diluted in dimethyl sulfoxide, and the final concentration of dimethyl sulfoxide was adjusted to be identical in each well, including the control.

Western Blot Analysis

After slices had been incubated for about 24 and 72 hr, they were rinsed with phosphate-buffered saline (PBS) and then homogenized in a sample buffer containing 2 mM EDTA, 2.3% sodium dodecyl sulfate (SDS), 10% glycerol, and 62.5 mM Tris (pH 6.9). After centrifugation at 15,000 rpm for 15 min, the supernatant was stored frozen at −20°C. Proteins were separated by SDS-polyacrylamide gel electrophoresis (10% acrylamide) and transferred electrophoretically to a nitrocellulose membrane. Blots were incubated with the primary antibody and subsequently with the secondary antibody, followed by development with an ECL kit (Amersham, Piscataway, NJ). Anti-GRP78 antibody (1:20,000) and anti-β-actin antibody (1:5,000) were used as the primary antibodies. The density of each band was measured with Image J software (National Institutes of Health, Bethesda, MD), and the relative band intensity was obtained as the density of Tm-treated band

divided by that of control band of each experiment after the adjustment by using corresponding density of β-actin band.

Immunohistochemistry and Immunofluorescence

For labeling of neurons in the spinal cord slices, cultures were fixed with 4% paraformaldehyde for 1 hr; rinsed with PBS; and, after blocking, stained overnight at 4°C with SMI-32 (1:2,500) or anti-calretinin antibody (1:5,000) diluted in PBS containing 0.3% Triton X-100 and 0.2% bovine serum albumin. After several washes with PBS containing 0.3% Triton X-100, the slices were incubated with secondary antibodies (1:250) for 5 hr and then visualized with diaminobenzidine tetrahydrochloride (DAB).

For immunofluorescence, the fixation procedure and primary antibodies were the same as described above, except that the two primary antibodies were used together for double staining. Incubation with the secondary antibodies (1:100), Alexa Flour 488 goat anti-mouse IgG and Alexa Flour 568 goat anti-rabbit IgG, was for 1 hr. Photographs were taken with a fluoroscope with a CCD camera (Nikon, Tokyo, Japan) and were colored with imaging software or were taken by using a confocal microscope (MRC-1024; Bio-Rad).

Definition of Viable Neurons and Statistical Analysis

Organotypic slice culture has the advantage of allowing both immunoreactivity and anatomical location to be assessed for accurate identification of cells. We defined viable motor neurons as SMI-32-positive cells with a large cell body (>30 μm) located in the anterior horn of the spinal cord, whereas dorsal horn interneurons were defined as anti-calretinin antibody-positive cells in the dorsal horn.

We counted the number of viable motor neurons and dorsal horn interneurons in each slice. The average number of viable cells in each slice was calculated, and the viability rate was obtained as the average number under each test condition divided by that in the control for every experiment. The experiments were repeated at least three times independently. Statistical analysis was perfomed by using the Kruskal-Wallis test, Welch's *t*-test, and Student's *t*-test with Microsoft Excel add-in software (Statcel 2).

RESULTS

Induction of ER Stress by Tm in Organotypic Slice Culture

Western blot analysis showed increased expression of GRP78 in slices incubated with 2 μg/ml Tm for 24 hr compared with control slices, and, even after 72-hr incubation with 1 μg/ml Tm, the increased expression of GRP78 persisted (Fig. 1). The GRP proteins are constitutively expressed in all cells, and their transcription is induced by a number of different stimuli that disrupt ER function (Kaufman, 1999). Among these proteins, GRP78 is the best characterized ER-stress marker and ER molecular chaperone, and it serves as a master regulator that plays an essential role in activating important transducers for initiation of the UPR (Zhang and Kaufman, 2006). Thus, this finding suggests that exposure to Tm caused ER stress in cultured slices of rat spinal cord.

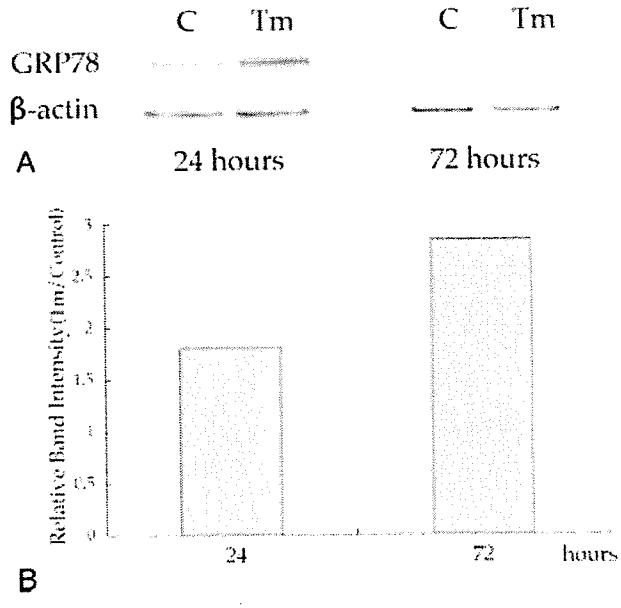

Fig. 1. Western blots showing increased expression of GRP78 in the Tm-treated group after 24 and 72 hr of incubation (**A**). Relative band intensity calculated from the densities of bands measured in Western blots (**B**). Increased GRP78 expression was shown to persist even after 72 hr of incubation. Tm, tunicamycin; C, control.

Toxicity of Tm for Spinal Cord Neurons

The viability rate of both motor neurons and dorsal horn interneurons decreased in a dose-dependent manner (Fig. 2), indicating that Tm was toxic for spinal cord neurons in organotypic slice culture. In addition, the viability rate of dorsal horn interneurons was considerably lower than that of motor neurons at the low concentration of Tm. These results suggest that dorsal horn interneurons were more highly susceptible to Tm-induced neurotoxicity.

Differing Effects of BFA and Tm on Spinal Cord Neurons

Although the number of slices was not sufficient for statistical analysis, motor neurons were more severely damaged than dorsal horn interneurons in BFA-treated slices (Fig. 2). This finding is consistent with the results of our previous study, which showed that motor neurons were more vulnerable to BFA-induced neurotoxicity in dissociated culture (Kikuchi et al., 2002). Both Tm and BFA are ER stress inducers, but they showed different profiles of spinal cord neuronal damage.

Protective Effect of PFT on Spinal Neurons Against Tm-Induced Neurotoxicity

When the slices were incubated concomitantly with Tm and PFT, a p53 inhibitor, the viability rate of dorsal horn interneurons showed a significant increase at 1, 2, and 10 μg/ml of Tm (Fig. 3), except when the